Climate Dynamics (1999) 15:451–473

B. Fontaine · Serge Janicot · P. Roucou

Coupled ocean-atmosphere surface variability and its climate impacts in the tropical Atlantic region

Received: 14 April 1998 / Accepted: 24 December 1998

Abstract This study examines time evolution and statistical relationships involving the two leading ocean-atmosphere coupled modes of variability in the tropical Atlantic and some climate anomalies over the tropical 120 °W–60 °W region using selected historical files (75-y near global SSTs and precipitation over land), more recent observed data (30-y SST and pseudo wind stress in the tropical Atlantic) and reanalyses from the US National Centers for Environmental Prediction (NCEP/NCAR) reanalysis System on the period 1968–1997: surface air temperature, sea level pressure, moist static energy content at 850 hPa, precipitable water and precipitation. The first coupled mode detected through singular value decomposition of the SST and pseudo wind-stress data over the tropical Atlantic (30 °N–20 °S) expresses a modulation in the thermal transequatorial gradient of SST anomalies conducted by one month leading wind-stress anomalies mainly in the tropical north Atlantic during northern winter and fall. It features a slight dipole structure in the meridional plane. Its time variability is dominated by a quasi-decadal signal well observed in the last 20–30 ys and, when projected over longer-term SST data, in the 1920s and 1930s but with shorter periods. The second coupled mode is more confined to the south-equatorial tropical Atlantic in the northern summer and explains considerably less wind-stress/SST cross-covariance. Its time series features an interannual variability dominated by shorter frequencies with increased variance in the 1960s and 1970s before 1977. Correlations between these modes and the ENSO-like Nino3 index lead to decreasing amplitude of thermal anomalies in the tropical Atlantic during warm episodes in the Pacific. This could explain the nonstationarity of meridional anomaly gradients on seasonal and interannual time scales. Overall the relationships between the oceanic component of the coupled modes and the climate anomaly patterns denote thermodynamical processes at the ocean/atmosphere interface that create anomaly gradients in the meridional plane in a way which tends to alter the north–south movement of the seasonal cycle. This appears to be consistent with the intrinsic non-dipole character of the tropical Atlantic surface variability at the interannual time step and over the recent period, but produces abnormal amplitude and/or delayed excursions of the intertropical convergence zone (ITCZ). Connections with continental rainfall are approached through three (NCEP/NCAR and observed) rainfall indexes over the Nordeste region in Brazil, and the Guinea and Sahel zones in West Africa. These indices appear to be significantly linked to the SST component of the coupled modes only when the two Atlantic modes + the ENSO-like Nino3 index are taken into account in the regressions. This suggests that thermal forcing of continental rainfall is particularly sensitive to the linear combinations of some basic SST patterns, in particular to those that create meridional thermal gradients. The first mode in the Atlantic is associated with transequatorial pressure, moist static energy and precipitable water anomaly patterns which can explain abnormal location of the ITCZ particularly in northern winter, and hence rainfall variations in Nordeste. The second mode is more associated with in-phase variations of the same variables near the southern edge of the ITCZ, particularly in the Gulf of Guinea during the northern spring and winter. It is primarily linked to the amplitude and annual phase of the ITCZ excursions and thus to rainfall variations in Guinea. Connections with Sahel rainfall are less clear due to the difficulty for the model to correctly capture interannual variability over that region but the second

B. Fontaine (✉) · P. Roucou
CNRS, Centre de Recherches de Climatologie,
Fac. Sciences Gabriel, B.P 138, F-21004 Dijon Cedex,
France
E-mail: fontaine@u-bourgogne.fr

S. Janicot
Météo-France, Laboratoire de Météorologie Dynamique du CNRS,
Ecole Polytechnique, F-91128 Palaiseau Cedex, France

Atlantic mode and the ENSO-like Pacific variability are clearly involved in the Sahel climate interannual fluctuations: anomalous dry (wet) situations tend to occur when warmer (cooler) waters are present in the eastern Pacific and the gulf of Guinea in northern summer which contribute to create a northward (southward) transequatorial anomaly gradient in sea level pressure over West Africa.

1 Introduction

In the tropics the atmospheric variability is rather weak and mainly driven by surface boundary conditions at large scales (Gill 1980). Consequently, the main modes of climate variability have often been described over the oceanic areas through objective statistical methods performed on sea-surface temperature anomalies (SSTA). Two quasi-global modes have been pointed out: (1) an El Nino/Southern Oscillation-like pattern in the tropics whose time coefficients have strong interannual variance; and (2) an extratropical mode opposing the southern parts of the global ocean to its northern parts whose time coefficients register longer term fluctuations (Folland et al. 1986; Kawamura 1994; Moron et al. 1995, among many others). The relationship between quasi-global SSTA and continental rainfall data has also been detailed in many diagnostic and model investigations (Palmer 1986; Ropelewski and Halpert, 1987, 1989; Semazzi et al. 1988, 1996; Wolter 1989; Ward et al. 1990; Ward 1992; Rowell et al. 1995; Trzaska et al. 1996, Janicot et al. 1998). All these studies provide consistent results highlighting the role of large-scale ocean-atmosphere interactions in the tropics.

Less agreement is found in studies focusing on the tropical Atlantic and its surrounding continents where climate variability is related more to processes of regional scale. The leading modes of Atlantic SSTA variability have been recognised for a long time, through different datasets and statistical techniques, as having their strongest loadings in the tropical basin (Servain et al. 1985). However two questions remain open. The first question concerns the reality of the interhemispheric mode associated with opposite SSTA in the northern and southern tropical parts of the Atlantic, featuring an 'Atlantic dipole' (Servain 1991). This topic has been regularly examined through principal component analyses performed on the tropical Atlantic SSTA observed on different periods (Lough 1986; Houghton and Tourre 1992; Zebiak 1993; Enfield and Mayer 1997). Such a spatial structure is not clearly seen before the 1950s but appears relevant mainly to the most recent and best documented period (Lough 1986). Second, Houghton and Tourre (1992) have shown that, even in recent years, the 'Atlantic dipole' was perhaps due to an artefact of the method, since it cannot be retrieved when a varimax orthogonal rotation is performed on the principal components. Third, Enfield and Mayer (1997) established that such meridionally antisymmetric behaviour is not a dominant characteristic of SSTA variability in the tropical Atlantic. The second question concerns the interannual variability in the equatorial and southeastern Atlantic which is well captured by the second SSTA mode but appears to be not self-sustained by dynamical and thermal processes over the Atlantic (Zebiak 1993). Such variability might be initiated by external forcings (Lanzante 1996) such those driving the warm and cold phases of the El-Nino-Southern-Oscillation (ENSO). Warm events in the tropical Atlantic have received much attention (Carton and Huang 1994) and various processes have been postulated to explain them. In particular, the 'apparent Atlantic Ninos' could be due to external forcings from the Pacific (Curtis and Hastenrath 1995) since significant increases (decreases) of the zonal component of the wind stress are linked to low (high) values of the Southern Oscillation Index (SOI) as shown by Delecluse et al. (1994).

Those questions are interesting because thermal anomaly gradients in the Atlantic are mostly meridional and hence linked to the timing and the vagaries of the rainy seasons on both sides of the equator and specifically over North Africa and South America. When the SSTA gradient points southward (northward) in northern spring and summer, abnormally dry (wet) July–September conditions tend to occur in the Sahel region (Tanaka et al. 1975; Lamb 1978a,b; Lamb and Peppler 1992; Hastenrath 1990; Druyan 1991; Fontaine and Bigot 1993; Fontaine and Janicot 1996; Janicot et al. 1998). When for example this gradient persists in southern spring and summer, abnormally wet (dry) February–April conditions tend to occur in the Nordeste region (Hastenrath and Greischar 1993; Nobre and Shukla 1996; Roucou et al. 1996). These fluctuations can be viewed as anomalies in the location of the Inter Tropical Convergence Zone (ITCZ) during the rainy season, an abnormal equatorward location being associated with dry rainfall anomalies in the Sahel. Consequently, the multimonth memory of the ocean should cause interseasonal persistence of the SSTA gradient and thus should maintain rainfall anomalies on both sides of the equator. This, however, does not clearly appear in the observations as noted by Shinoda (1989), Lau and Sheu (1991) and Semazzi et al. (1996) among others, who provide evidence of 6 month lags in rainfall anomalies in North and South Africa linked to the ITCZ seasonal migration (i.e. abundant rainfall in 1950 and the reverse in 1973). Additionally rainfall time series in the Nordeste and South Africa regions do not present any negative trend or interannual persistence similar to the North Africa rainfall time series.

This study is not a review of the key phenomena that control surface temperature and rainfall in the Atlantic region. It concentrates on the question of the

relationship between interannual modes of climate variability in the tropics and Atlantic regional climate anomalies detected in surface conditions and provides some examples of rainfall impacts at regional scale. It focuses on the tropical Atlantic region to examine the statistical relationship between ocean-atmosphere interactions in the Atlantic, and the observed and US National Centers for Environmental Prediction (NCEP/NCAR) anomaly patterns. This approach involves both historical files and data from the NCEP/NCAR reanalysis System.

2 Mean seasonal cycle and interannual patterns

The observed surface conditions in the tropical Atlantic are investigated through the SST and surface pseudo-wind stress datasets objectively analysed using a Cressman scheme and first investigated by Servain et al. (1985) and Servain (1991). The data used here come from a more recent version available on a 2°lat. * 2° long. grid over the tropical Atlantic domain (30°N–20°S from 60°W to the coast of Africa) for the period 1964–1996 on a monthly time-step.

2.1 Mean seasonal cycle

In the tropical Atlantic the seasonal cycle forces a quasi-regular reversing of SSTs and of meridional components of the wind stress, featuring an inter hemispheric gradient. Its mean seasonal excursion has been often described (Hastenrath and Lamb 1977; Hastenrath 1984) and is portrayed by 3-month periods in Fig. 1. The relatively strong annual cycle and the presence of warmer waters north of the equator have been shown to result from interactions between SSTs and the meridional stress (Chang 1996). Basically, the confluence zone, which separates the northern and southern trade wind systems, is mainly located on (or slightly northward of) the warmest SSTs. Its southernmost position is reached in January–March when warmer (colder) waters lie in the Guinea Gulf (in the northern tropics) and its northernmost location in July–September. This makes these two areas very sensitive when abnormally warm (cold) waters occur during the cold (warm) season. Notice that relatively cold waters are encountered all along the year in the central equatorial Atlantic (Fig. 1), which, for similar reasons, makes this band especially sensitive to SST anomalies. Location of

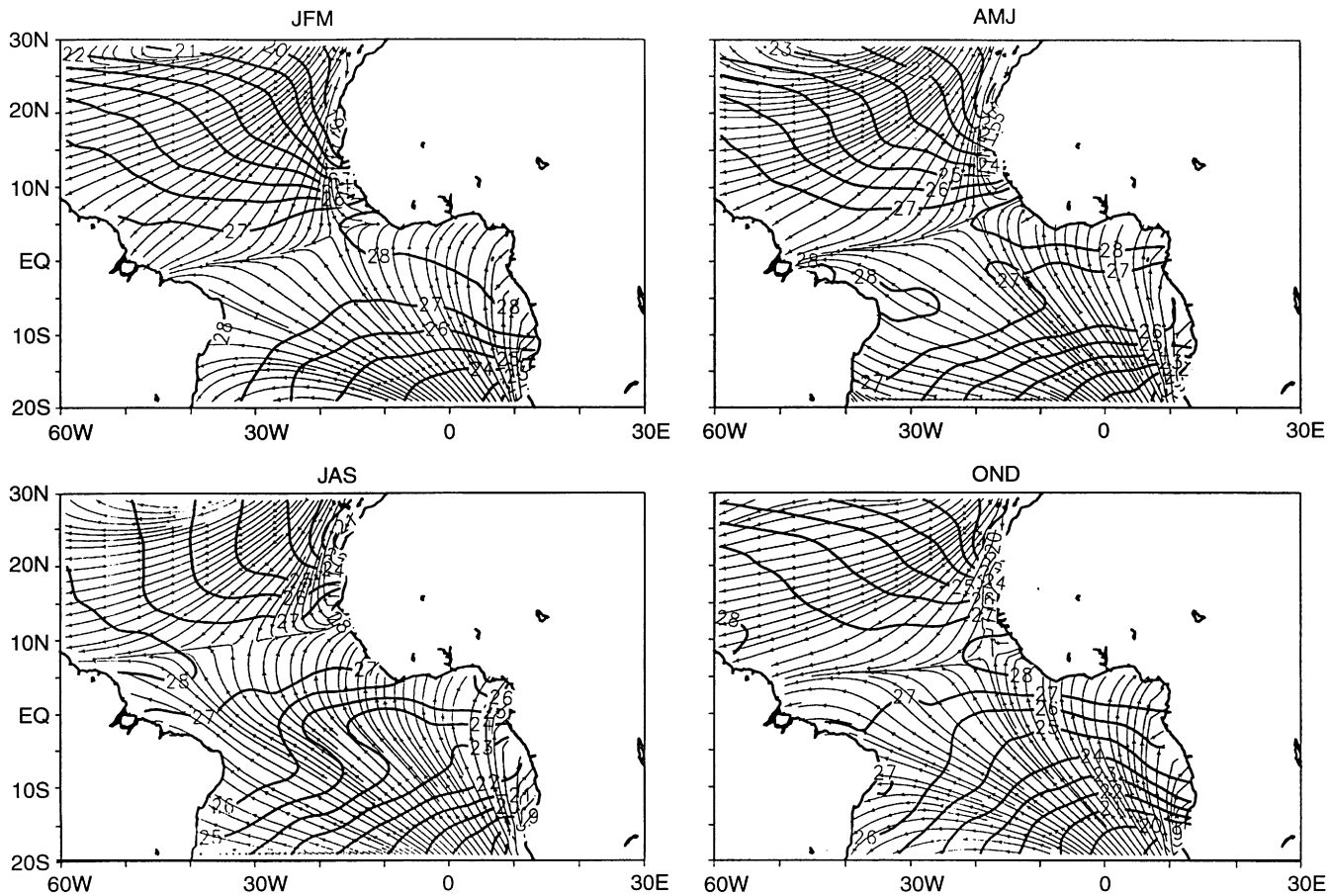

Fig. 1 Mean 3-month seasonal sea surface temperatures (°C) and streamlines of the mean seasonal surface pseudo-wind stress for the period 1964–1995: January–March (*JFM*), April–June (*AMJ*), July–September (*JAS*) and October–December (*OND*)

the equatorial 'cold tongue' corresponds to divergence in the surface wind stress associated with the diffluence area which separates the southern easterlies blowing to the west and the monsoon veering towards the African continent, stronger in northern spring and summer. From April to June, the latitudinal location of the confluence zone near the equator and the presence of warm waters ($>28\,^{\circ}$C) in the western equatorial Atlantic (Hastenrath and Lamb 1977) also favours stronger easterlies and hence equatorial upwelling coupled with a westward gradient of sea surface topography. In fact, the equatorial Atlantic registers rather strong seasonal fluctuations of SSTs. This is due to the Ekman divergence/pumping at the ocean-atmosphere interface, stronger in northern spring and summer over that region, and to positive feedbacks involving stratus clouds: lower SSTs tend to strengthen the atmospheric inversion and hence to produce more stratus clouds which lower SSTs as shown by Philander et al. (1996).

2.2 Interannual coupled variability

Singular value decomposition (SVD) analyses of SST and wind-stress monthly anomalies from January 1964 to December 1995 are provided to document the main ocean-atmosphere modes of interannual variability (patterns and time-coefficients) in terms of associated parts of variance. SVD is a generalisation of the diagonalisation procedure performed in principal component analysis to matrixes that are not square as shown in Bretherton et al. (1992). SVD of the cross-covariance matrix between SST and wind stress monthly anomalies has been performed to identify pairs of spatial patterns that maximise the mean-squared temporal covariance between these two fields. It has been computed using a complex matrix for the wind stress information with the zonal/meridional components as the real/imaginary parts. Both original monthly anomalies and linearly detrended monthly anomalies series have been used: in the first case, the seasonal mean cycle has been removed but not the linear trend 1964–1997; in the second case, both have been removed. Figures 2 and 3 respectively present the homogeneous spatial structures (in units of correlation coefficients) and the standardised time-coefficients associated with the two leading coupled modes obtained with detrended data to focus mainly on the interannual variability and for the sake of stationarity. Following Wallace et al. (1992), the homogeneous correlations show the spatial patterns whose polarity and amplitude of the corresponding expansion coefficients are represented. Together they account for 33% and 20.3% of the total variance, respectively for the SST and pseudo-wind stress anomalies (SSTA and PWSA).

Figure 2 (top) allows us to depict the first coupled mode with strong positive values of SSTA associated with strong southwesterly wind stress anomalies north of $5\,^{\circ}$N. This coupled mode will be called hereafter TW1 (for temperature and wind stress) whereas TWt1 (TWw1) will denote time series of the temperature (wind stress) patterns. The sign reversal in the equatorial and southern tropical Atlantic indicates a slight dipole structure between $15\,^{\circ}$N and $15\,^{\circ}$S but clearly dominated by the north tropical Atlantic. There is a tendency for SSTA of negative sign to occur south of the equator but reduced in area and with weaker wind anomalies in the northern tropical Atlantic. This could be due to the fact that any wind-SSTA singular value decomposition will tend to polarize the SSTAs with respect to a dominant transequatorial anomaly pattern: a northward interhemispheric wind anomaly is linked to positive/negative SSTA north/south of the equator. In fact, no dipole structure appears when the data are not detrended. In this case (not shown), stronger weights are also registered in the PWSA field in the northern parts of the tropical Atlantic with no clear counterpart in the Southern Hemisphere. These results conform well to the conclusions of Houghton and Tourre (1992) who showed that during the 1964–1988 period SSTAs north and south of the ITCZ are not significantly correlated and that there is no temporally coherent or out-of-phase fluctuations in each hemisphere. Our coupled patterns explaining 16.9% and 13.8% of the SSTA and PWSA variances respectively have a squared covariance fraction of 67% and a normalised squared covariance of 14% (scf/ncf in Fig. 3): scf is useful for comparing the relative importance of modes (Bretherton et al. 1992); ncf is useful to compare the strength of the relationship between the two data fields and ranges from zero if the fields are unrelated to 1 if they are perfectly correlated (Wallace et al. 1993). TW1 is dominated by the thermal and wind stress variability in the northern tropical basin. Their time-correlated series ($r = 0.67$ when the atmosphere leads the ocean by one month) present a time variability dominated by a quasi-decadal signal, more obvious with SSTAs (Fig. 3). The lag of one month in the atmosphere-ocean relationship is consistent with Carton et al. (1996) but somewhat shorter than two months, as reported by Nobre and Shukla (1996) for the period 1964–1987.

The second coupled mode (called hereafter TW2) refers to the second coupled pattern in Fig. 2. It exhibits positive values of SSTA between $30\,^{\circ}$N and $15\,^{\circ}$S with stronger weights in the $5\,^{\circ}$N–$15\,^{\circ}$S band (16.1% of explained variance) associated with northeasterly wind stress anomalies (6.5%) in the equatorial and southern areas of the tropical basin and with southerly anomalies in the tropical north Atlantic ($30\,^{\circ}$N–$10\,^{\circ}$N). Notice also the diffluence zone between these two areas. TW2 has a squared covariance fraction of 12% and a normalised covariance of 6%. The two time-correlated series (Fig. 3) are less correlated ($r = 0.52$ when the atmosphere leads the ocean by one month)

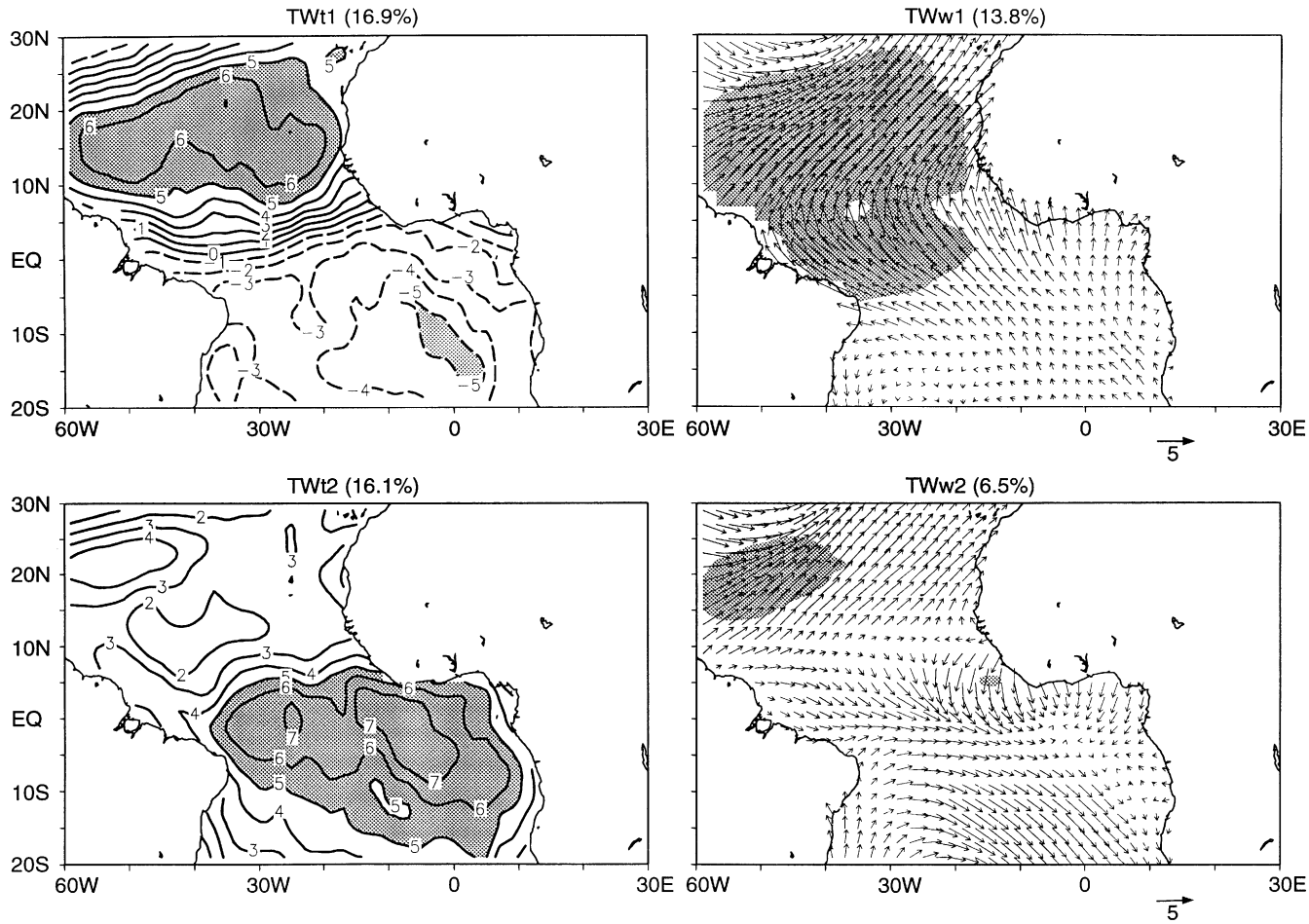

Fig. 2 The two leading SVD monthly coupled temperature-wind-stress (TW) surface patterns for the period 1964–1995 in units of correlation coefficients (*100) with *shading* when the absolute values exceed 0.5 (25% of explained variance): TWt and TWw refer to the temperature-side and wind-side coefficients of TW modes, respectively. The value at each grid point is equivalent to the temporal correlation between the expansion coefficients of one mode (the homogeneous SVD fields) and the TW field at the same grid point

than TW1 and both series have an interannual variability dominated by shorter frequencies.

The patterns in Fig. 2 express a local coupling between PWSA and SSTA (Huang et al. 1995). The statistical association increases when PWSAs lead SSTAs by one month, and is stronger over the area where trade winds are rather stable. In fact, intraseasonal interactions between wind stress and the one month-lagged SST are slightly modulated by the mean seasonal cycle as shown in Table 1 and Fig. 4. The linear time correlations be tween the PWSA–SSTA expansion coefficients (Table 1) are stronger from April to September ($r = 0.84$ with TW1; $r = 0.65$ with TW2) and are not significant in southern summer (JFM) for TW2 ($r = 0.39$). Correlations with other climatic indices (NAO, SOI, Nino3) are low and not significant.

The mean seasonal evolution of field-correlations in Fig. 4, where each season is considered within the all month analysis (Figs. 2, 3), allows us to get more information. TW1 is clearly dominated by significant loadings north of 5 °N (positive shaded values for SSTAs associated with stronger southwesterly PWSAs). This arises particularly in northern autumn and winter (OND and JFM) when the northern trade winds are normally stronger (and hence when local SSTAs are very sensitive to PWSAs) in agreement with Nobre and Shukla (1996). Notice first that there is no convergence of the wind stress field over the warmest SSTAs (positive shaded area); second, the significant negative SSTA counterpart south of the equator has always smaller extent, except perhaps in April–June when the northern (southern) weights weaken (strengthen). In their analysis of SST variability in the tropical Atlantic, Carton et al. (1996) provide numerical evidence that the interhemispheric SSTA pattern mostly results from low-frequency changes in evaporation due to the effect of wind variations on both shorter and longer time scales. Our results allow us to add that the quasi-decadal variations in the trans-equatorial SSTA gradient (Figs. 3,5) could be also forced by wind-stress changes due to the mean seasonal cycle (Fig 4).

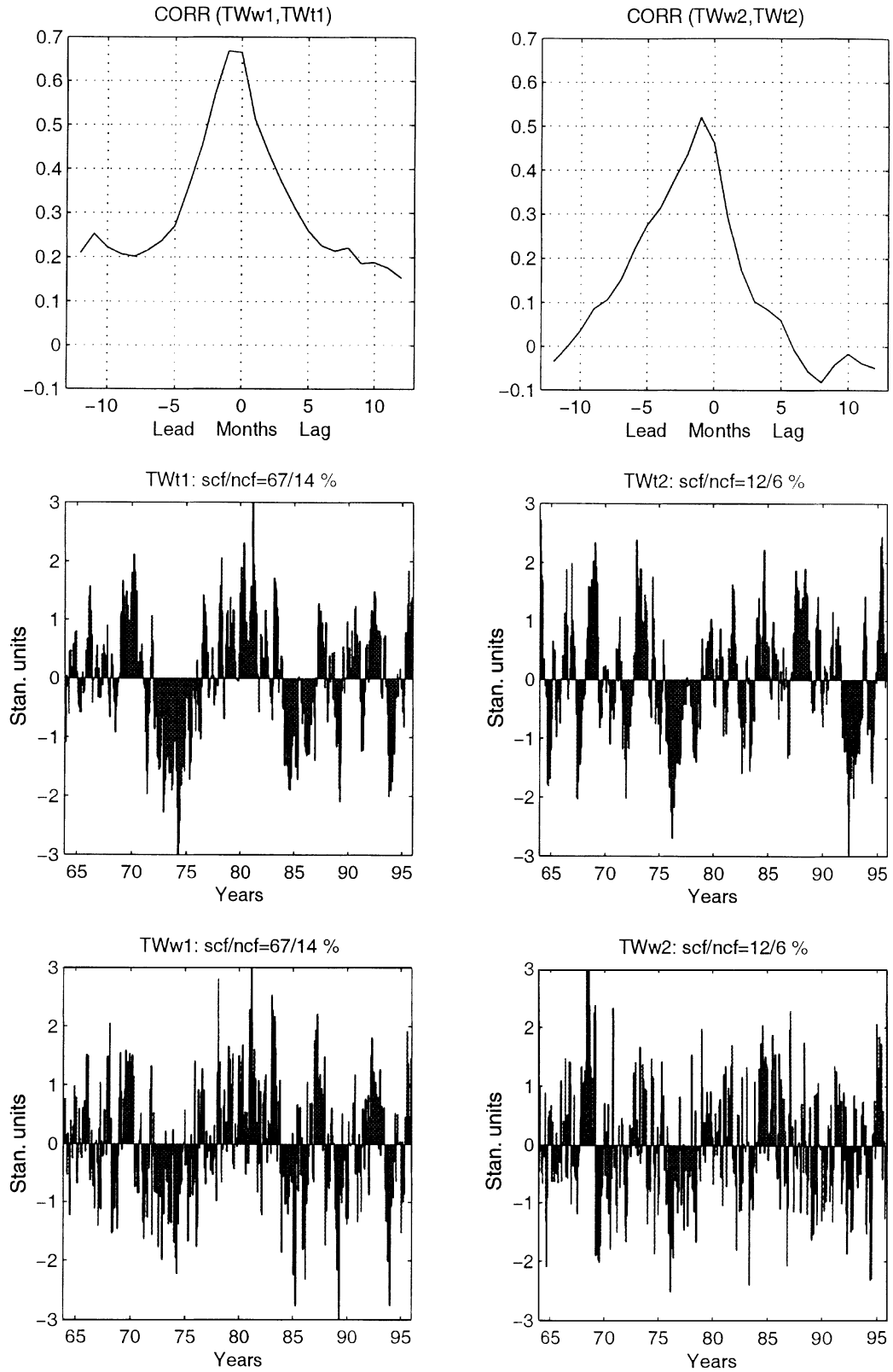

Fig. 3 Time variability of the monthly expansion coefficients of the 2 SVD modes (*TW1* at left) in standardised units for the period 1964–1995: (*upper*) lead-lag correlations between the PWSA and SSTA time-coefficients (PWSA leads SSTA by one month at maximum correlation; values on the X-axis are expressed in months); (*middle and lower*) the SSTA and PWSA monthly time series with the squared covariance fraction (*scf*)

Table 1 Linear correlation coefficients (*100) on a 3-month basis between the 1964-1995 time-series of the two leading SSTA coupled modes in the Atlantic and some atmospheric and oceanic indicators (see the text). Asterisks indicate the significant values at $P = 0.05$ when taking into account the autocorrelation functions of time-series

	TWt1			
	JFM	*AMJ*	*JAS*	*OND*
TWw1	+ 80*	+ 84*	+ 86*	+ 72*
NAO	− 48	− 04	+ 08	− 30
SOI	− 35	− 23	− 24	+ 01
Nino3	+ 24	+ 35	+ 22	+ 03
	TWt2			
	JFM	*AMJ*	*JAS*	*OND*
TWw2	+ 39	+ 65*	+ 65*	+ 60*
NAO	+ 24	− 20	− 22	− 09
SOI	− 17	+ 09	− 06	− 06
Nino3	+ 26	− 09	− 02	+ 13

By contrast, the strongest TW2 loadings (Fig. 4, bottom) extend mainly south of 5N from April to December (during the southern cold seasons) with positive SSTA areas and PWSA convergence onto the equatorial band (Fig. 4). When in January-March (during the northern cold season) the near-equatorial convergence of wind stress anomalies disappears, higher local correlations can be found in the tropical north Atlantic (near 20–25 °N and 40–50 °W) between enhanced southwestern PWSAs and warmer SSTAs.

These results conform well to the conclusions of Enfield and Mayer (1997) and Enfield et al. (1998). The strongest correlations of the two leading coupled modes are concentrated over specific areas (near 15 °N for TW1 and near 5 °S–10 °S for TW2). Mainly located in one hemisphere, they have only slight values of opposite sign in the other. This could be due to the fact that wind-stress mean seasonal patterns over the tropical Atlantic tend to force SSTs in a way that creates meridional gradients across the equator. In any case, the similarity between mean seasonal SST structures and interannual SSTA patterns indicate a close relationship between the interannual variability and changes in timing and magnitude of the seasonal cycle as previously noted by Moura and Shukla (1981). In particular, TW1 is clearly dominated by the north tropical Atlantic from October to March when northeasterlies are stronger (Fig. 4, top). In fact the negative SSTA correlations south of the equator are always less significant than their northern counterpart and the OND structure does not display any significant dipole pattern: TW1 mainly expresses the variability of the meridional SSTA gradient in the vicinity of the ITCZ due to PWSA-SSTA interactions in the north tropical Atlantic (Fig. 4, top). By contrast, TW2 expresses the variability of the equatorial (but also tropical south) Atlantic, mainly from April to December when PWSA convergence and westerly anomalies clearly occur near the equator (Fig. 4 bottom). In JFM however, when the northern (southern) trade winds are reinforced (vanish), the values increase in the north (significant near 20–25 °N) but decrease in the south. These results show that TW2 is linked to wind-stress anomalies involving the two Atlantic basins but registers stronger variance in the 10 °N-10 °S equatorial band. Thus warmer (cooler) waters in the quasi-equatorial zone could be supplied from the north-western and/or the south-western tropical Atlantic in response to the relaxation (strengthening) of the trade winds, which also conforms well to the numerical experiments conducted by Carton et al. (1996).

3 1919–1994 Non stationarities

The two SSTA patterns have been projected onto the MOHSST dataset of the UK Meteorological Office (Bottomley et al., 1990) in order to consider longer time evolutions of these SSTA structures along with their robustness and stability. This observed SST file is used for the period 1919–1994 in a gridded version where the data have been corrected for observational bias and analysed over a 5 °lat. * 5 °long. grid. Figure 5 (top and middle) shows the monthly expansion coefficients and fluctuations longer than 7 y using a Butterworth filter (Murakami 1979) over the 76-ys period 1919–1994. Both series have the sign of SSTA in their respective regions of highest loadings, north and south of the ITCZ for TW1 and TW2 respectively. For comparison, Fig. 5 (bottom) presents an ENSO-like index defined over the central equatorial Pacific (Nino3; 90 °W–150 °W; 5 °N–5 °S). The two Atlantic time series (TWt1,2) present a rather stable high-frequency variability over the whole period and the intermonthly variance does not increase after 1964 (the beginning of the period on which SVD calculations are made). By contrast, low-frequency fluctuations clearly increase after the beginning of the 1970s in the TW1 and TW2 series. In particular, the strong quasi-decadal fluctuations in TW1 series observed on the last 20–30 ys are not reported before, except perhaps in the 1920s and 1930s, but with shorter periods. In any case the slow TW1 fluctuations are less obvious in the 1940s, 1950s and 1960 s, when the intermonthly variability seems to be stronger for TW2 in the southern and equatorial Atlantic and for Nino3 in the central equatorial Pacific (Fig. 5 middle and bottom). This agrees with our previous results (Fontaine et al. 1998): low frequency variability of surface oceanic parameters in the tropical Atlantic during the last 20 ys differs from the preceding period. One can notice for example that TW2 variance is clearly enhanced just before the slow post-1977 warming.

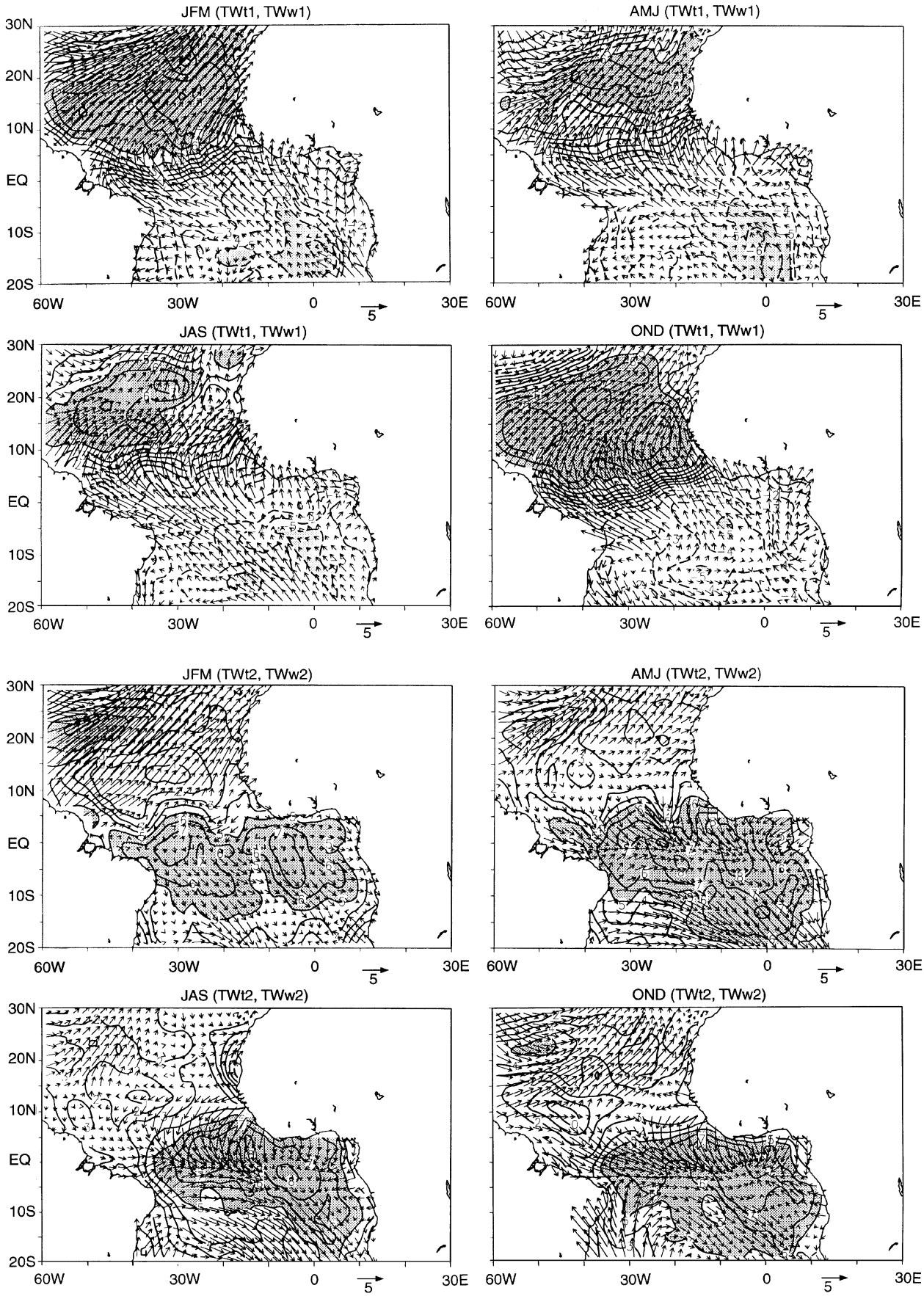
JFM (TWt1, TWw1)
AMJ (TWt1, TWw1)
JAS (TWt1, TWw1)
OND (TWt1, TWw1)
JFM (TWt2, TWw2)
AMJ (TWt2, TWw2)
JAS (TWt2, TWw2)
OND (TWt2, TWw2)
30N
20N
10N
EQ
10S
20S
60W
30W
0
30E
5

4 Associated surface patterns

In this section, we investigate two basic atmospheric variables (surface air temperature and sea level pressure) through the available NCEP/NCAR dataset, for the period 1968–1994. The NCEP/NCAR dataset (Kalnay et al. 1996) consists of a reanalysis of the global observational network of meteorological variables (wind, temperature, geopotential height, humidity on pressure levels, surface variables, and flux variables like precipitation rate) with a "frozen" state-of-the-art analysis and forecast system to perform the data assimilation throughout the whole period 1958–1997. This circumvents inhomogeneities in previous numerical analyses due to changes in techniques, models and data assimilation. Data are reported on a 2.5×2.5 degrees grid every 6 h (00.00, 06.00, 12.00, 18.00 UTC) on 17 pressure levels from 1000 hPa to 100 hPa.

We will focus on the anomaly patterns associated with the two SSTA Atlantic modes and with Nino3. Both lead/lag correlation and lead/lag composite analyses on the intermonthly and interseasonal time scales have been used. The results are not dependent on the techniques and the significant lags are shorter than three months, therefore only some examples of synchronous correlations are reported here on a seasonal (3 month) basis.

4.1 Surface air temperatures

Figure 6 displays the January–March (JFM) and the July–September (JAS) correlation structures relative to surface air temperatures (Ta) from 40 °N to 40 °S between 120 °W and 60 °E in order to consider the subtropics and significant portions of the Indian and Pacific Oceans. TW1 and 2 are strongly correlated with the tropical Atlantic at regional scale, that is over its northern and southern areas respectively, due to the strong correlation between surface air and sea surface temperatures over oceanic areas at seasonal time scales. Taking into account sign conventions in Fig. 2, positive TW1 values in Fig. 6 (top) correspond to warmer/cooler Ta lying north/south of the mean ITCZ location in the Atlantic (and the reverse for negative values) associated in JFM with cooler temperatures north of 25 °N in the eastern Atlantic. This is in agreement with the 136-y EOF analysis (1856–1991) of Enfield et al. (1998) who found significant coherence with antisymmetric phase in the 8–12 y band during the northern winter and spring. Positive TW2 (Fig. 6, middle) correspond to warmer temperatures all over the Atlantic but particularly south of 10 °N (and the reverse for negative values). This differs from the correlation structures (not shown) obtained when more local indices are considered. For example, when one defines two thermal indexes, one over the northern tropical Atlantic (30 °N–5 °N), and another over the southern and equatorial Atlantic (5 °N–20 °S), which are the key-areas of the two Atlantic modes, no clear and significant 'dipole' correlation pattern can be found. This conforms to the idea that TW1 can be thought in terms of transequatorial anomaly gradients conducted by PWSA–SSTA interactions over the tropical north Atlantic while TW2 points out a transequatorial same-sign relationship dominated by the equatorial and tropical south Atlantic.

The relationship with Nino3 (Fig. 6, bottom) concerns the tropical Pacific equatorward of latitutde 20° and appears stronger during northern winter: strong positive values are located in the eastern tropical Pacific, and in JFM, over the Indian Ocean and the American and African continents. The Atlantic basin is less involved. When lagged relationships are considered (not reported here) a weak reversing of correlation values in the tropical Atlantic appears in JAS, as a result of positive lagged correlations linking temperatures in the eastern Pacific and the northern tropical Atlantic one to two seasons later. The larger extent of the significant values in northern winter is also retrieved when other global indicators (like SOI) are used in place of Nino3. In fact the recent interannual SST fluctuations in the tropical North Atlantic are influenced by Nino3 related anomalies (Fig. 6, bottom-left) and hence by their ENSO-Pacific component (Harzallah et al. 1996) but do not stress any strong and consistent signal at regional scale. The lack of synchronous relationship linking Nino3 (Fig. 6, bottom) and SSTA in the southern and equatorial Atlantic during the JAS season has been confirmed through composite analyses. This is also consistent with the low synchronous relationships linking the two Atlantic modes to the atmospheric/oceanic Pacific indices (SOI and Nino3) as reported in Table 1: low (high) SOI, as warm (cold) Nino3 episodes are synchronous with positive (negative) TW1 and 2 values mainly in northern winter. This means in particular that, over the recent period, low SOI and warm episodes in the Pacific are linked first to a northward thermal anomaly gradient crossing the equator which forces some cooling to the south (positive TW1), and second to a warm forcing in the equatorial and southern tropical basin (positive TW2). This tends to diminish the amplitude of thermal anomalies in the equatorial and south Atlantic since Nino3 (and negative SOI, Table 1) are weakly associated with positive values of both TW1 and TW2. The lagged southern winter cooling south of the equator following ENSO events (positive correlations with

Fig. 4 Seasonal fields of TW1 and TW2 expressed in units of linear correlation coefficients (*100) for the January–March (JFM), April–June (AMJ), July–September (JAS) and October–December (OND) seasons: *TWt1,2* with *shading* when the absolute values of the homogeneous correlations exceed 0.5 (25% of explained variance) as in Fig. 2; *TWw1,2* (*vectors*) are superimposed

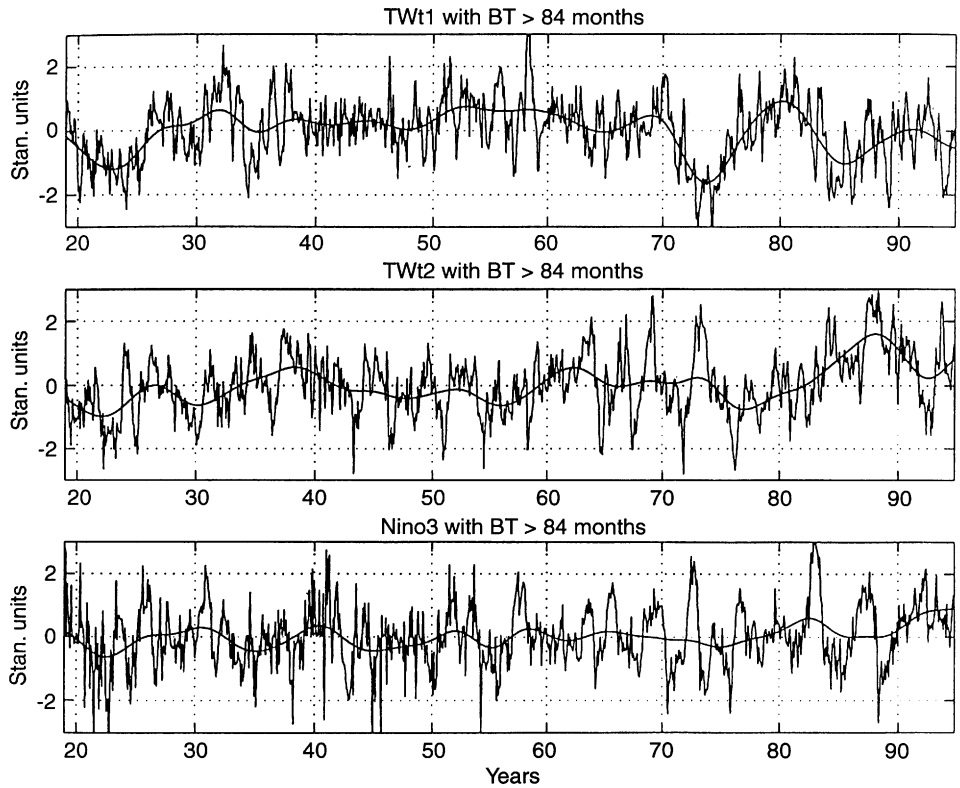

Fig. 5 Time-coefficients of the two tropical Atlantic SST patterns after projection onto the MOHSST SST dataset for the period 1919–1994 along with low frequency fluctuations (periods > 84 months) using a recursive Butterworth (BT) filter

Nino3) and the small 'obscuring effect' of the overall ENSO response are also attested by Enfield and Mayer (1997) and Enfield et al. (1998), respectively.

4.2 Sea level pressures

Over the tropical Atlantic, SSTAs are associated with thermodynamical processes involving the atmosphere. This can be illustrated through linear correlations using the JFM and JAS values of the observed SVD modes and the NCEP/NCAR sea level pressure (SLP) fields as in Fig. 7, where the low SLP zone associated with ITCZ is superimposed. When the thermal anomaly gradient points northward in the Atlantic (positive TW1) during southern summer (JFM) an abnormal southward SLP anomaly gradient generates a northward pressure force and hence the transequatorial winds from the southern tropics already seen in Figs. 2, 4. All these features cannot be really observed in northern summer (JAS), in particular the southerly PWSAs south of the equator (Fig 4), since no clear transequatorial SLP anomaly gradient associated with TW1 occurs during this season: Figure 7 (top-right) presents only increasing SLP anomalies south and over the ITCZ. Change in correlations on both sides of the low SLP zone signals a thermodynamical control of SSTAs by surface winds. This conforms to the numerical results of Carton et al. (1996) that indicate that SST dipole structures are primarily controlled by surface wind stress in the Atlantic with a quasi-decadal variability (also observed in Fig. 3). The connection involving TW2 (Fig. 7 middle) is limited to the southern and equatorial parts and no dipole structure can be found. The JFM and JAS patterns are in agreement with the mean seasonal cycle (Fig. 1), particularly the northward excursion of the greater loadings: when warmer waters occur in the southern Atlantic (positive TW2) surface pressures are lower than normal. This means southward anomalies of the pressure gradient force and hence winds across the equator (Fig. 4, bottom).

According to the empirical results of Wagner (1996) and to the model results of Chang et al. (1997) we hypothesise that such an anomalous northward wind-stress anomaly could maintain surface pressure anomalies of opposite sign over the northern and southern parts of the Atlantic. This evolves into south-easterly (south-westerly) anomalies in the Southern (Northern) Hemisphere because of the Coriolis force as shown by the TW1 correlation structures in Figs. 2, 4, 6, 7. This tends to reduce (enhance) the trade winds prevailing in the north (south) as shown in Fig. 1 and to create thermal and SLP anomalies in the Atlantic as shown in Figs. 6, 7: the surface heat flux into the Atlantic could increase (decrease) through a reduction (an enhancement) of evaporation caused by decrease (increase) in surface wind-stress leading to warmer (cooler) temperature and lower (higher) pressure in the

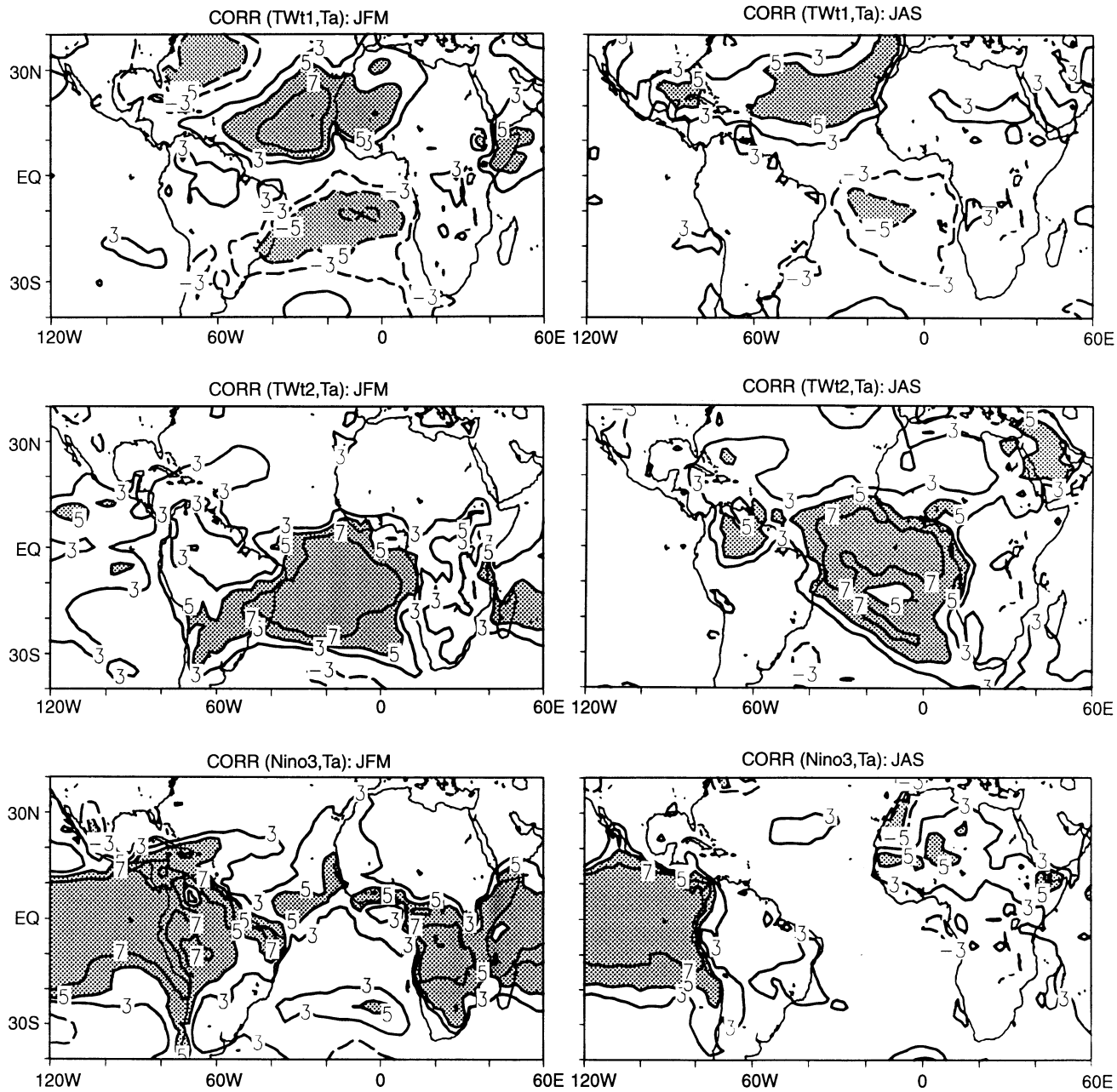

Fig. 6 Linear correlations between the three selected oceanic modes and surface air temperatures (*Ta*) from the NCEP/NCAR analysed dataset in January–March (*JFM*, *left*) and July–August (*JAS*, *right*) for the period 1968–1994. Positive/negative values above of 0.3 ($\sim 10\%$ of common variance) in *solid*/*dotted* lines (every 0.2). *Shading* denotes the areas where the values exceed 0.5 in absolute value (25%), which is the significance level at $p = 0.05$ for 14 effective degrees of freedom

low atmospheric levels. The reinforcement of initial cross-equatorial thermal and pressure gradients strengthens in turn the cross-equatorial wind-stress anomalies. So despite their statistical independence by construction over the whole tropical Atlantic and the whole year, positive TW1 and TW2 are associated with inverse wind anomalies near the ITCZ (northward for TW1 and southward for TW2) in agreement with the mean seasonal cycle (mainly in JFM for TW1 and in JAS for TW2).

So, in the vicinity of the ITCZ, wind stress anomalies associated with TW1 and TW2 tend to create opposite SSTA just northward and southward of the low SLP zone. This explains the tendency for SSTA in the two basins to be out of phase on each side of the ITCZ and is the reason why dipole structure emerges when using surface air temperatures and sea level pressures, two ITCZ sensitive variables. The TW1 correlation fields shown in Figs. 6, 7 register also significant seasonal variations in both structure and intensity. The TW1

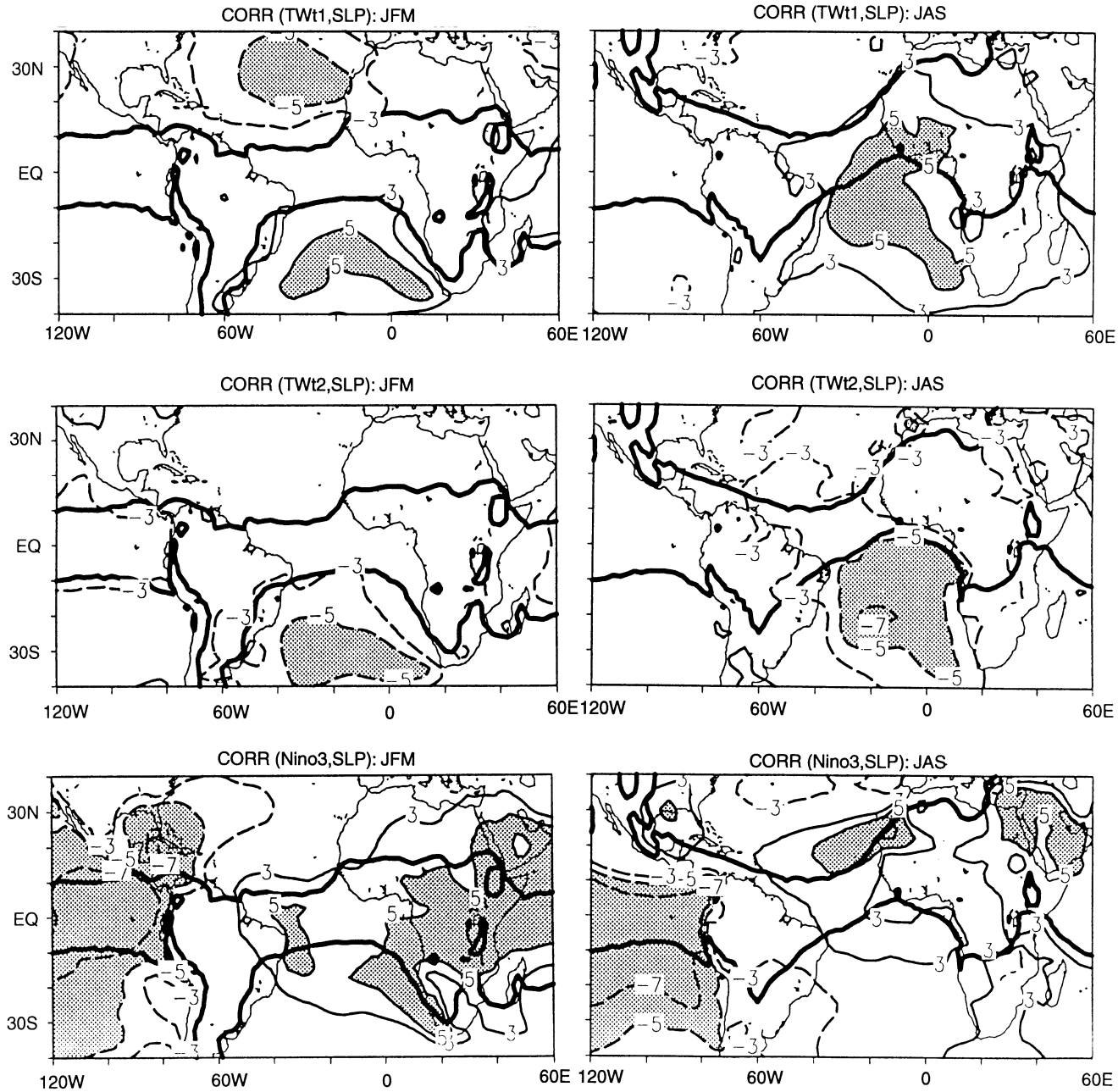

Fig. 7 As in Fig. 6 but for sea level pressures (*SLP*): The *heavy solid lines* superimposed join the points where mean SLP values = 1013 hPa in JFM and 1012 hPa in JAS

results appear to be consistent with the non-dipole character of the tropical Atlantic surface variability at the interannual time-step and over the period 1968–1994, but they show that this oceanic mode is associated with surface thermodynamics in the meridional plane over the Atlantic in a way which tends to alter the mean seasonal cycle and hence produce excursions of the intertropical convergence zone (ITCZ).

The patterns relative to Nino3 (Fig. 7 bottom) are very different. Pressure increases east of 60 °W, over the South American (mainly in JFM) and African continents. In northern winter (JFM), one can notice negative values in the eastern Pacific and the northern tropical Atlantic west of 60 °W along with positive values eastward. In northern summer the positive values are north of 15 °N. So when warmer waters occur in the global tropics (positive Nino3) the associated pressure anomaly gradient over the tropical Atlantic points eastward in JFM and north-eastward in JAS (meaning an enhancement of the trades) due to the seasonal migration of positive pressure anomalies

over Africa. These Nino3 related correlation are in agreement with the results of Latif et al. (1997, their Figs. 8 and 12) who notice the presence of warmer waters, higher surface pressures and stronger southeasterlies in the equatorial and southern Atlantic during Nino3-warm related phases in northern winter.

5 Associated moist static energy and precipitable water contents in the atmosphere

This section examines the NCEP/NCAR moist static energy (MSE) and precipitable water (PW) contents in the atmosphere associated with the three observed modes of variability to complement the previous surface results.

5.1 Moist static energy content

Low-level atmospheric motions are related to SSTA patterns because SSTs affect the position of convection through the moist stability (Philander 1990). MSE does not measure the total energy in the atmosphere but takes into account the main forms of static energy (the kinetic energy is negligible) per unit mass: geopotential, enthalpy, latent energy. We will consider MSE in the low atmospheric levels (at 850 hPa).

$$\mathrm{MSE} = gz + CpT + Lq,$$

where gz is the gravitational-potential energy, with g the gravitational acceleration and z the geopotential height of the 850 hPa isobaric surface;
CpT is the enthalpy, with Cp the specific heat of dry air at constant pressure ($Cp = 1000\ \mathrm{m^2\,s^{-2}\ deg^{-1}}$) and T the temperature (Kelvin) of the 850 hPa isobaric surface;
Lq is the latent energy associated with evaporation and condensation of water, with L the latent heat of evaporation ($L = 2501$ J/g) and q the specific humidity of the 850 hPa isobaric surface (further details in Philander 1990).

Figure 8 presents the MSE correlation patterns at 850 hPa associated with the three oceanic modes along with the region where MSE exceeds 327 J (superimposed heavy solid lines). The TW1 patterns (Fig. 8, top) confirm the results obtained with the surface air temperature (Fig. 6 top): they are clearly dominated by the tropical north Atlantic (near 20 °N) in JFM (positive values) with two inverse counterparts (negative values) south of the equator and to the north. Positive TW1 values correspond to greater (lesser) energy content at 850 hPa north (south) of the mean ITCZ location in the Atlantic and, in JFM, to a MSE decrease north of 25 °N in the eastern Atlantic (and the reverse for negative values). This is however consistent with a less (a more) southward location of the largest MSE in JFM. The TW2 structures are also in agreement with the previous sections, in particular the location of the highest values south of the seasonal MSE maxima and their seasonal migration. Positive (negative) TW2 values denote a less (a more) northward MSE excursion in northern summer over the Atlantic. The Nino3 results are similar to those obtained with surface air temperature (Fig. 6 bottom): they mainly concern the tropical zone and appear stronger during northern winter. However, the Atlantic basin is more involved. In particular, during the northern summer (JAS) warm (cold) Nino3 episodes are synchronous with stronger (lesser) energy content into the MSE maximum zone over the Atlantic (near 10 °N) and the Sahel zone in Africa (near 15 °N). These differences denote the role of evaporation/condensation processes.

5.2 Precipitable water amount

The amount of precipitable water (PW) at the surface is a measure of the vertically integrated moisture (g/kg) the atmospheric column contains in a unit area (m^2). More exactly, PW represents the amount of liquid water that would result if all the water vapour in the unit column of the atmosphere were condensed (in g/m^2 or in mm). The spatial distribution of the annual-mean PW (Peixoto and Oort 1992; Fig. 12.3 p. 280) shows a decrease of PW from the equatorial oceanic areas ($> 40\ g/m^2$) to the high latitudes ($< 25\ g/m^2$ near 45 °N and 40 °S on the Atlantic). PW is hence linked to the main thermodynamical processes involving the climate system in the tropics. Figure 9 displays the related January–March (JFM) and the July–September (JAS) TW1, 2 and Nino3 correlation structures along with the zone where PW exceeds 39 mm (heavy solid line) which features the ITCZ.

The positive TW1 values (Fig. 9 top) are mainly linked to wetter (drier) situations on the southeastern (northwestern) edges of the Azores high pressure cell in JFM (when it is more intense) and to wetter (drier) ones on the northern (southern) edges of the St. Helena high pressure cell in JAS (when it is more intense). This means more available PW content near ITCZ over the Atlantic–Africa region and less in the subtropics during the winter hemisphere (and the reverse for negative TW1). These patterns are consistent with the other correlation structures already presented (Figs. 4, 6–8). Notice however the northwestward gradient between the south tropical zone (negative values) and the PW maxima over the South American continent consistent with a less southward migration of PW maxima during the south tropical rainfall season meaning less available water vapour in the atmospheric column.

The positive TW2 values (associated with equatorial and southern abnormal warmings) are correlated with wetter conditions in the St. Helena high pressure area (Fig. 9 middle) and on the southern edge of the ITCZ in

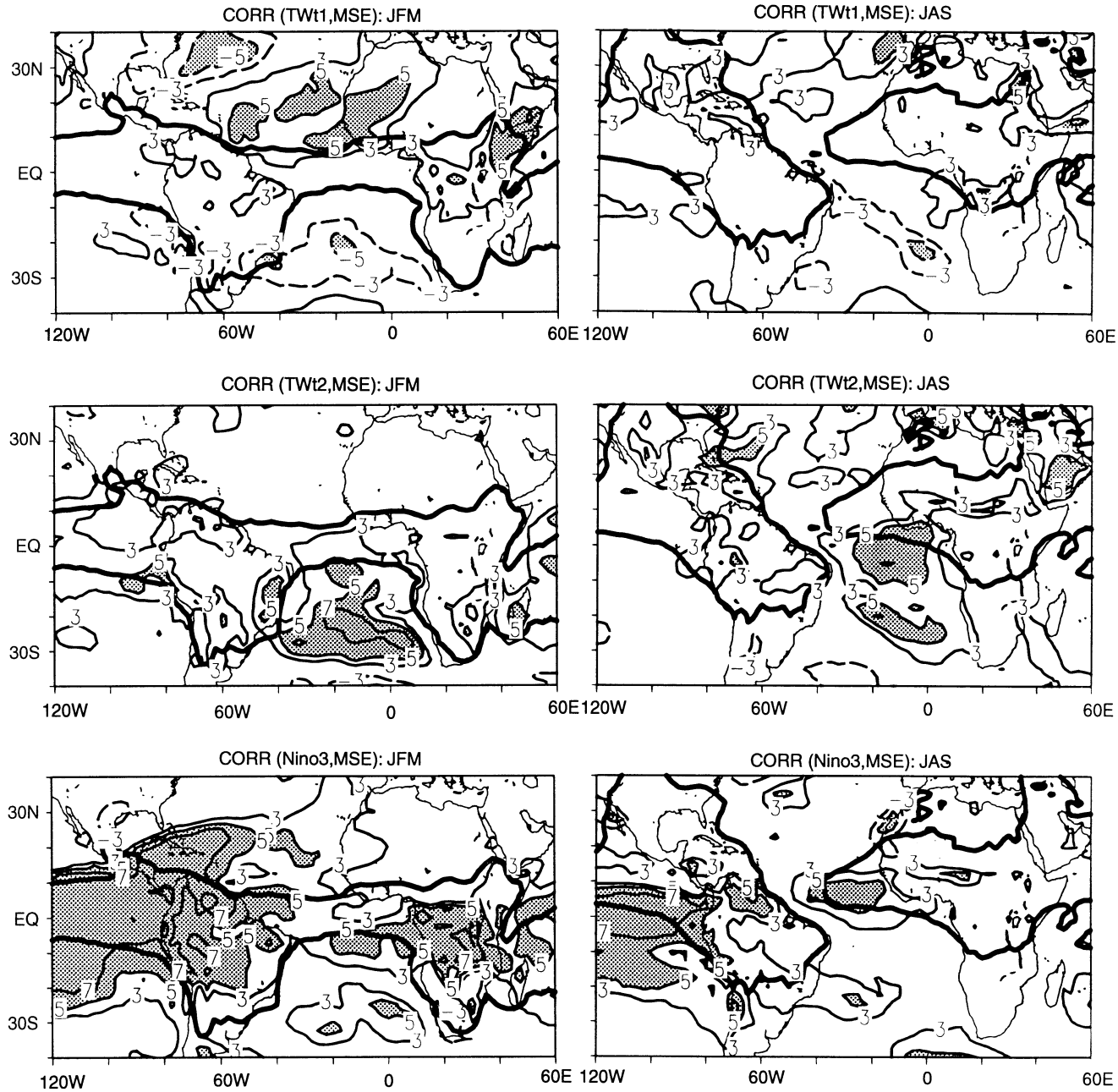

Fig. 8 As in Fig. 6 but for moist static energy (MSE) content at 850 hPa. The *heavy solid* lines superimposed join the points where mean MSE values = 327 J

JAS (and the reverse for negative TW2). This is in good agreement with the previous NCEP/NCAR results relative to surface air temperatures and sea level pressures (Figs. 6, 7), but also with the SVD patterns involving observed sea surface temperatures and winds (Fig. 4 bottom) from another dataset: they clearly show converging wind-stress anomalies over warmer waters in that region.

The Nino3 results are also coherent with the previous sections. Notice however in JAS a southwestward PW gradient between the African Sahel (negative correlations) and the PW near-equatorial maxima in the Atlantic (positive correlations) compatible with a less northward migration of PW maxima during the monsoon season. This means less available water vapour in the atmospheric column over the Sahel during the rainfall season.

This requires examining the relations in terms of NCEP/NCAR and observed seasonal rainfall amounts.

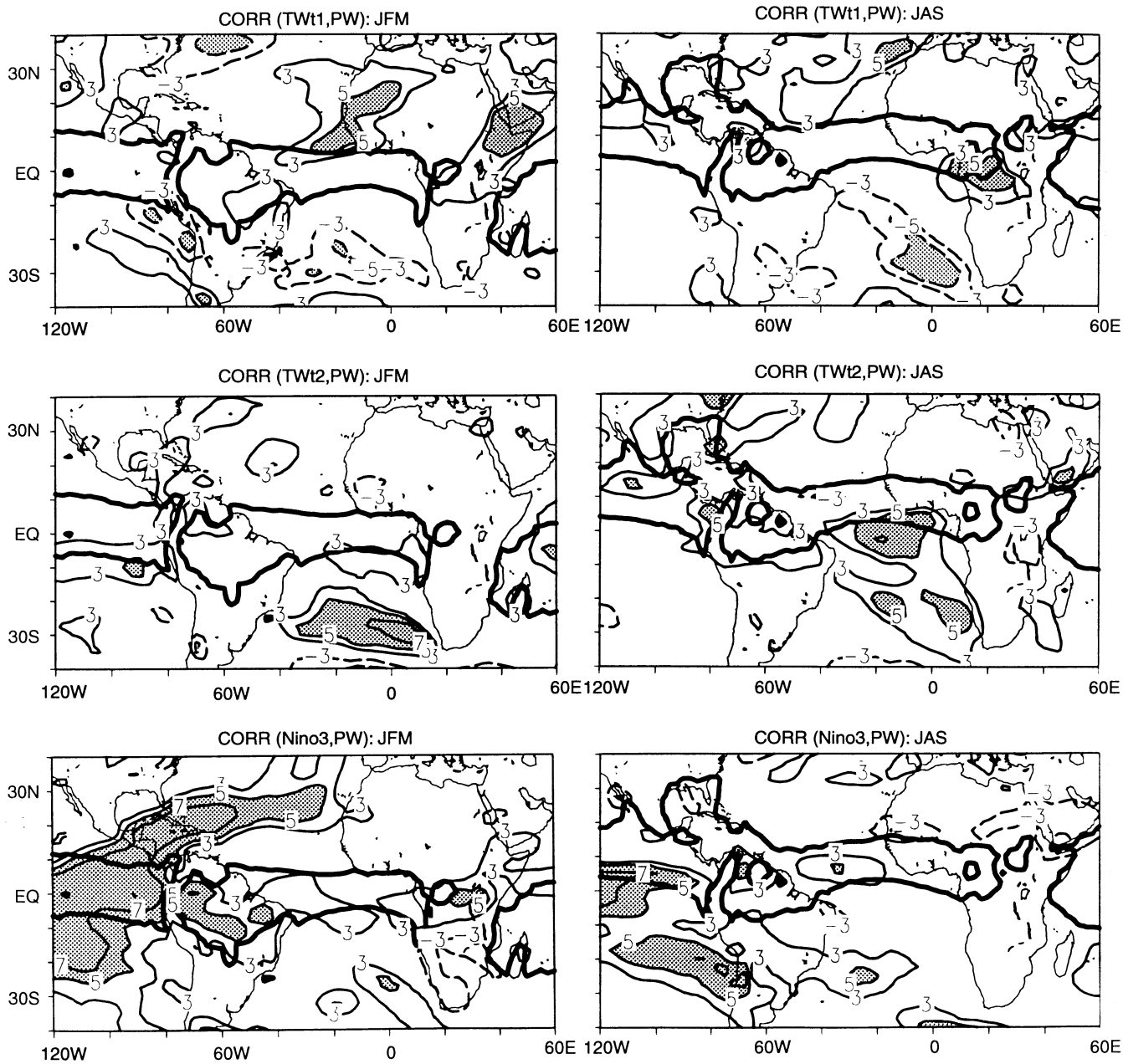

Fig. 9 As in Fig. 6 but for precipitable water (PW) content at the surface. The heavy solid lines superimposed join the points where mean PW values = 39 g/m^2

6 Associated NCEP/NCAR precipitation amounts

6.1 Continental observed versus NCEP/NCAR rainfall indexes

There are no observations affecting directly the variable 'precipitation' in the reanalyses, so the NCEP/NCAR rainfall indexes have first to be compared with those that can be computed in the observations. A recent study by Trenberth and Guillemot (1998) provided evidence that there are substantial biases in the NCEP/NCAR precipitation in terms of mean values and interannual variability. This arises especially over the oceanic areas and, in particular, in the central Pacific. So we will only focus on some continental areas using the global land gridded data developed specifically for model validation by Hulme and Jones (1993) in a recent version with a 2.5 °lat. * 3.75 °long resolution on the 1968-1996 period. Seasonal modulation of continental rainfall at regional scale is approached through NCEP/NCAR and observed rainfall indexes

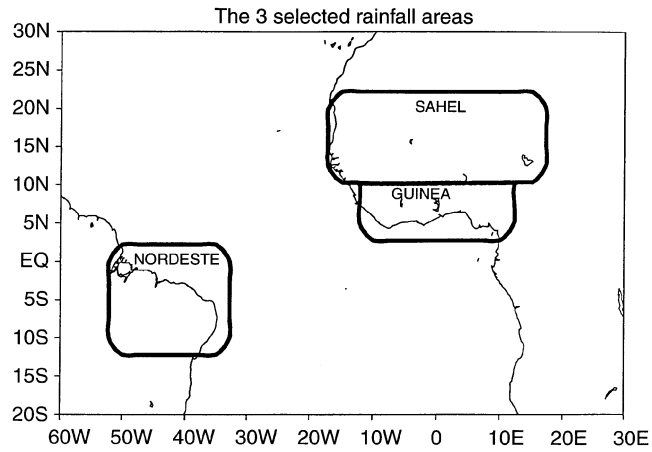

Fig. 10 The three selected continental areas defining the continental rainfall indexes: *Sahel*, *Guinea* and *Nordeste* from north to south

defined by areal averages over three selected regions. From south to north we define a South American region centred on Nordeste region in Brazil (10 °S Eq; 50 °W–35 °W) and called hereafter Nordeste; a subtropical West African region centred on the Guinea shore (4 °N–9 °N; 10 °W–10 °E) and called Guinea; a sub-Saharan region centred on the Sahelian belt (10 °N–20 °N; 15 °W–15 °E) and called Sahel. These regions (Fig. 10) have been selected because they experience strong seasonal contrast in rainfall on both sides of the equator and of the Atlantic basin.

Figure 11 presents the NCEP/NCAR and observed mean monthly rainfall amounts (left) along with the interannual time evolution of cumulated NCEP/NCAR and observed rainfall (right) during the respective rainy seasons: January to May in Nordeste, June to October in Sahel and Guinea. Notice first the rather good similarity between the observed (solid) and NCEP/NCAR (dashed) mean monthly values (Fig. 11, left) on the period 1968–1996, in particular with the Sahel indexes. However, when compared to the observations, the NCEP/NCAR indexes underestimate (overestimate) by about 50 mm the monthly amounts in Nordeste and Guinea during their respective rainfall (dry) seasons. This is consistent with a smaller latitudinal range for the simulated ITCZ latitude and its associated rain band over the Atlantic and its surrounding continents. This also conforms to the results of Trenberth and Guillemot (1998, their Figs. 5, 6) who showed a more equatorward location of the rain band over the Atlantic, both in annual and northern summer mean situations. To better compare the interannual variability of cumulative rainfall amounts (Fig. 11, right), the linear correlations between model and observations (along with the first-rank autocorrelations of the time series used as a measure of interannual persistence) are also provided in Table 2. Notice first the rather good agreement in Nordeste and Guinea, although the NCEP/NCAR series have stronger interannual persistence, and second, the lower association at interannual time scale for Sahel contrasting with what is observed in terms of monthly mean values (Fig. 11, left). This reflects the difficulty for the reanalysis to produce correct rainfall anomalies in a region where strong meridional rainfall gradients exist: in Table 2 correlations decrease in the vicinity of the mean latitudinal location of the rain band from June to October, the lowest value being ($r = 0.39$ by 10 °N); they increase northward ($r = 0.50$ by 15 °N) and southward ($r = 0.80$ by 5 °N).

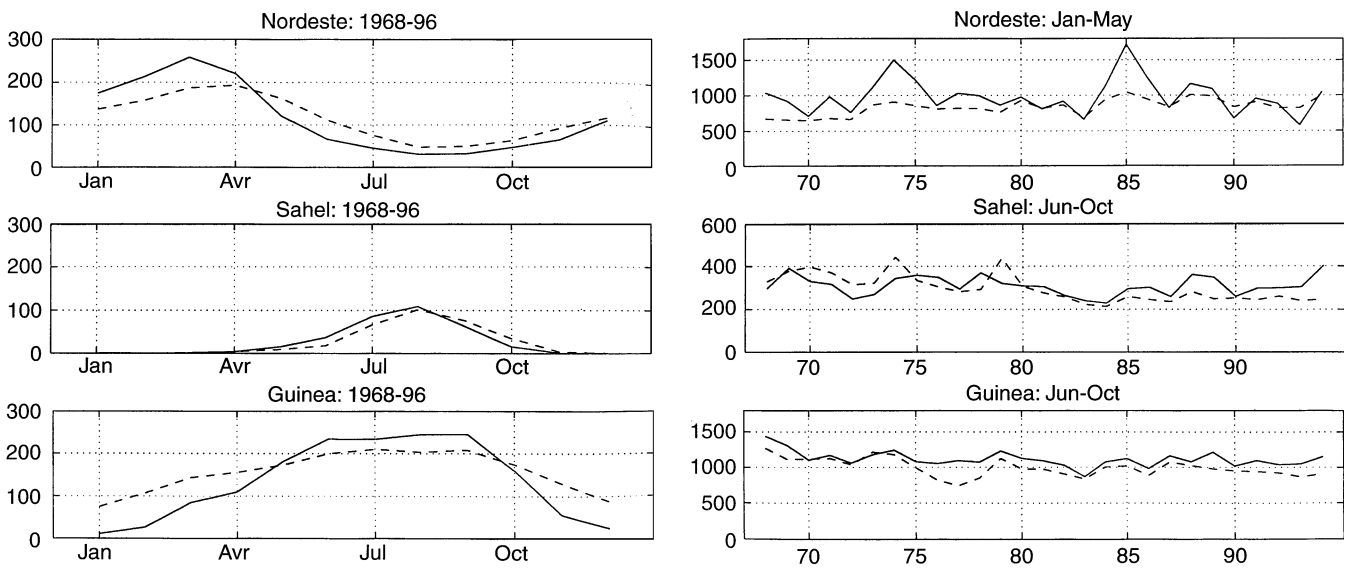

Fig. 11 *Left*: NCEP/NCAR (*dashed*) and observed (*solid*) mean monthly rainfall amounts (mm); *right*: NCEP/NCAR (*dashed*) and observed (*solid*) interannual evolution of cumulated rainfall (mm) over the three selected areas during the rainy seasons: January–May for Nordeste; June–October for Guinea and Sahel

Table 2 Linear correlation (R) coefficients (*100) between the 1968–1994 time series of modelled and observed regional rainfall indexes on a 5-month basis, and their respective first rank autocorrelation coefficients (R1). The 3 terms on the left refer to a South American region centred on Nordeste in Brazil (10 °S-Eq; 500 °W–350 °W), a sub-Saharan region centred on the Sahelian belt (10 °N–20 °N; 15 °W–15 °E) and a West African region centred on the Guinea shore (4 °N–9 °N; 10 °W–10 °E). Asterisks denote the significant values at $P = 0.05$, taking into account the serial correlations in the time series

	R Modelled versus observed	R1 Modelled	R1 Observed
Sahel (June–October)	+ 39	+ 60	+ 26
Guinea (June–October)	+ 74*	+ 55	+ 29
Nordeste (January–May)	+ 61	+ 51	+ 23

Figure 12 shows the NCEP/NCAR rainfall amounts stratified over the nine strongest positive (solid bars) and the nine strongest negative (shaded narrow bars) seasonal values of the three oceanic modes during the common period 1968–1994. The strongest positive TW1 values (meaning warmer north Atlantic waters) are associated with decreasing rainfall over the three continental regions (significant in Nordeste during the main rainfall season), whereas the strongest positive Nino3 (warmer conditions in the central equatorial Pacific) coincide with significantly drier conditions after the main rainy seasons from July to September in Nordeste and after September in Guinea, that is during the poleward and equatorward excursions of the rainbelt, respectively. Nobre and Shukla (1996) have already observed that the main reason for rainfall deficiency (excess) in Nordeste is the early (later) withdrawal of the ITCZ towards the Northern Hemisphere. Hence, Nino3 and TW1 have similar links with NCEP/NCAR rainfall anomalies over the three selected areas. In the opposite sense, the strongest positive TW2 values (meaning warmer waters over the south-equatorial Atlantic) introduce north/south contrasts since they are clearly associated with significant wetter conditions in Nordeste from April to December and with significantly drier situations in West Africa: in AMJ and OND in Guinea; in AMJ and JAS over the Sahel. This points to an inverse tendency in rainfall between South America and West Africa linked to the south-equatorial mode which could explain the negative correlation ($r = -0.47$) between the Nordeste and Sahelian rainfall amounts when cumulated on their respective rainy seasons. Following Enfield (1996) we think that a significant part of the Atlantic SSTA has a direct association with rainfall, rather than being merely an indirect proxy for Pacific ENSO linkages.

Table 3 displays the 'multiple' correlations obtained when the NCEP/NCAR and observed rainfall indexes, for the seasons which register more than 150 mm (Fig. 10), are expressed as a linear function (regression equation) of the three observed oceanic modes. The values point out rather strong relationships, even with the model outputs, since in AMJ and JAS more than 50% of variance are explained with the Nordeste NCEP/NCAR indices, and more than 40% with Guinea in OND. The fact that all the coefficients tend to reinforce after the peak of the respective rainfall seasons conforms to the preceding remarks. Notice also the enhancement of these statistical associations during (or somewhat after) the heart of the rainfall seasons when observations are used: $r = +0.85$ with Nordeste and $r = +0.63$ with Guinea in April–June; $r = +0.66$ with Sahel in July–September. By comparison, the 'individual' (not displayed) correlations, which express rainfall as a function of only one oceanic mode, are all significantly lower. This suggests that thermal forcings upon continental rainfall are sensitive to particular linear combinations of the oceanic structures shown in Figs. 2, 6 which is in agreement with many previous model and empirical results. For example, if one considers the Sahel, Palmer (1986) and Rowell et al. (1990) show that, given observed SSTs as boundary conditions, atmospheric general circulation models can attain significant skill in simulating some contrasted rainfall seasons. However, simulations in which the SSTs are geographically restricted are less skillful than simulations with the full global SST field. Moreover, when considering longer time scales the empirical analyses of Ward and Hoskins (1996) show that 1949–1988 changes in the tropical Atlantic are particularly strong in July-September; in particular the 1969–1988 reduced Sahel rainfall imply a substantial reduction in cross-equatorial flow associated with a weakened and/or southward-shifted ITCZ over the eastern Pacific, Atlantic and Indian longitudes.

To provide more information about the relative and independent effects of the three oceanic modes the contemporaneous partial correlations (pc) relative to the observed rainfall indexes in AMJ (Nordeste and Guinea) and JAS (Sahel) are listed in Table 4. Notice the inverse values of the coefficients for TW1 and TW2 showing that the three rainfall amounts are linked to meridional anomaly gradients in the Atlantic involving both TW1 and TW2. In this context, the Atlantic mode whose key-area is located in the opposite hemisphere (the Southern Hemisphere for Sahel and Guinea and the northern one for Nordeste) has always greater weight. Guinea is primarily associated with TW2 ($pc = -0.52$): cold (warm) SSTAs in the equatorial and tropical south Atlantic are linked to abnormally dry (wet) situation. For Nordeste TW1 ($pc = -0.46$) leads the relationship: northward (southward) thermal anomaly gradients dominated by warm (cold) SSTAs in the tropical north Atlantic are synchronous of dry (wet) rainfall anomalies. Sahel however here appears more linked to Nino3 ($pc = -0.58$): the warm (cold) episodes in the central equatorial Pacific are synchronous of dry (wet) rainfall anomalies.

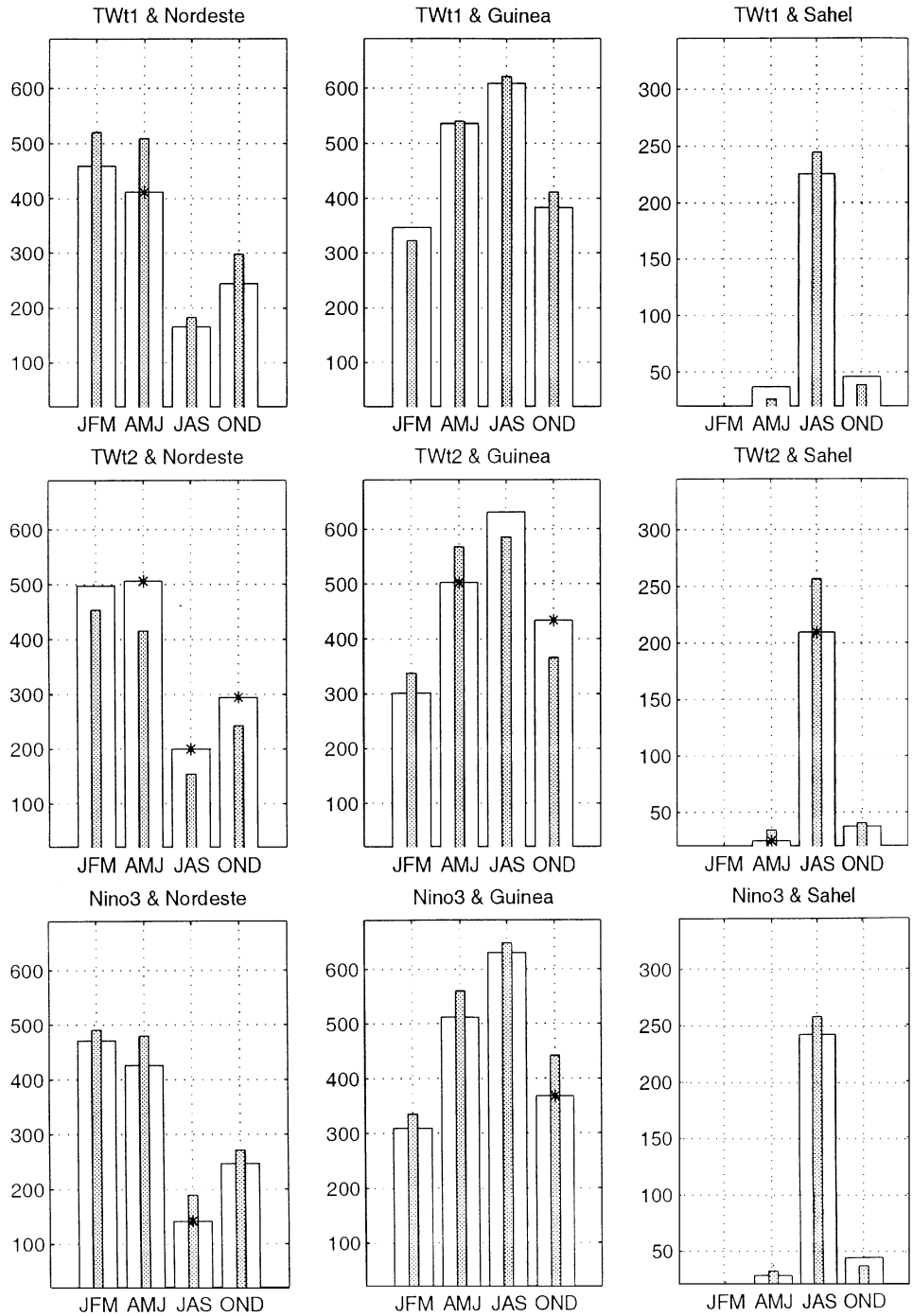

Fig. 12 Mean seasonal NCEP/NCAR rainfall amounts (mm) stratified over the 9 strongest positive (*solid bars*) and the 9 strongest negative (*shaded narrow bars*) seasonal values of the three oceanic modes during the common period 1968–1994. *Asterisks* denote the significant differences at $P = 0.05$ using a paired t-test. In April-June, for example, the *solid* (*shaded*) bars refer to: 1969-70-78-79-80-81-82-83-87 (1971-72-73-74-75-84-86-89-94) for TWt1 1969-73-84-87-88-89-90-91-93 (1970-71-72-75-76-78-81-82-92) for TWt2 1969-72-82-83-87-90-91-92-93 (1968-70-71-73-75-78-84-85-88) for Nino3

6.2 Oceanic and continental correlation patterns

Here we consider the intertropical correlation fields (20 °N–20 °S) obtained with the NCEP/NCAR rainfall amounts to produce the basic structure over the oceanic domain in AMJ and JAS (Fig. 13): the heavy solid lines denote areas where rainfall amounts exceed 100 mm/month. The TW1 / rainfall correlations display a northward gradient crossing the equator in AMJ (Fig. 13, top) meaning that warmer waters north of the

Table 3 Multiple linear contemporaneous correlation coefficients (*100) between the 1968–1994 time-series of the three selected SSTA modes and the modelled and observed regional rainfall indexes over Nordeste, Guinea and Sahel during the seasons when they exceed 150 mm. Asterisks denote the significant values at p = 0.05, taking into account the serial correlations in the time series

	Modelled				Observed			
	JFM	AMJ	JAS	OND	JFM	AMJ	JAS	OND
Sahel			+ 50				+ 66*	
Guinea	+ 45	+ 37	+ 42	+ 65*	+ 25	+ 63*	+ 42	+ 47
Nordeste	+ 33	+ 77*	+ 72*	+ 54*	+ 37	+ 87*	+ 41	+ 48

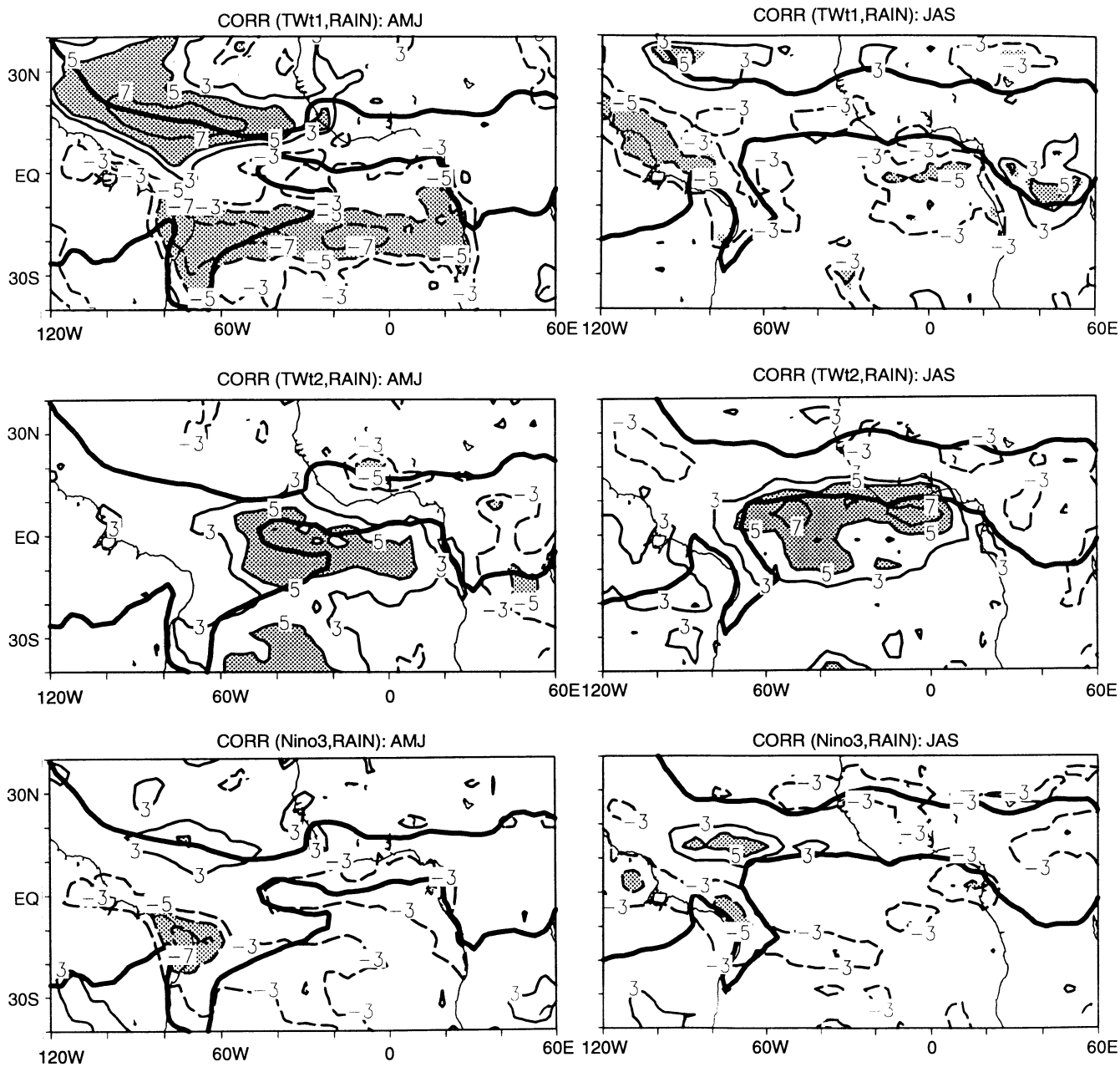

Fig. 13 As in Fig. 6 but for rainfall amounts (RAIN). The *heavy solid* lines superimposed join the points where mean RAIN values = 100 mm/month

Table 4 Partial correlation coefficients (*100) between the 1968–1994 time-series of the three SSTA modes and observed seasonal rainfall indexes in Nordeste (AMJ), Guinea (AMJ) and Sahel (JAS)

Observed	TWt1	TWt2	Nino3
Sahel (JAS)	+ 18	− 25	− 58
Guinea (AMJ)	+ 26	− 52	+ 08
Nordeste (AMJ)	− 46	+ 19	− 33

equator (positive TW1) are associated with positive/negative rainfall anomalies north/south of the rain belt over the Atlantic (and the reverse for cooler waters). This is consistent with the results of previous sections: abnormal southerlies blow from the southern tropics where the pressure is reinforced towards the northern Atlantic basin which experiences lower than normal pressure values (Figs. 2, 4, 7). The negative TW1/Nordeste relationship observed in Table 4 and Fig. 11 concerns in fact the entire 5 °S–15 °S zone. The TW2 / rainfall correlations (Fig. 13, middle) are positive (negative) in the vicinity of the southern (northern) edge of the rainfall maxima meaning that warmer waters positive over the equatorial and southern Atlantic are linked to wetter (drier) conditions just southward (northward) of the main rain band. On the African continent, correlations are mainly negative which is also consistent with Figs. 2, 4, 7. The correlation field related to Nino3 (Fig. 13, bottom) shows negative values along the American shore, and in JAS over the African Sahel. However, by contrast with those relative to the two Atlantic modes (Fig. 7, top, middle) and consistent with the lack of thermal relationship illustrated in Fig. 6 (bottom), no large area of rainfall correlation is registered over the Atlantic Ocean.

These results show the strong sensitivity of NCEP/NCAR seasonal rainfall to the meridional thermal and mass gradients in the Atlantic caused by the two Atlantic modes. When the southern (northern) tropical Atlantic is warmer than normal, the simulated ITCZ tends to move later towards the north (south) that is in April (September) in place of March (August).

7 Discussion and conclusion

Relationships between the leading modes of climate variability in the tropics and climate anomalies in surface conditions over the tropical Atlantic and its surrounding continents have been pointed out using both observed data (near global SSTs and precipitation over land, SST and wind stress in the tropical Atlantic) and selected outputs from the NCEP/NCAR reanalysis system for the last thirty years: surface temperatures, sea level pressure, moist static energy at 850 hPa, precipitable water at the surface and rainfall. Singular value decomposition analyses of observed SST and wind stress monthly anomalies from 1964 to 1995 capture the two leading ocean-atmosphere modes of interannual variability in the tropical Atlantic. Together they account for 33% and 20.3% of the total SST and wind stress variances respectively, with greater percentages in the 30 °N–10 °N and 5 °N–15 °S latitudinal bands. The first Atlantic mode (TW1, squared covariance fraction of about 67%) appears to be associated with thermodynamical processes at the interface, mainly in winter over the northern tropical basin, the wind stress anomalies leading SSTA by one month. It also presents a slight dipole structure in the meridional plane with multi-annual variability dominated by a quasi-decadal signal. Therefore, it can be mainly thought in terms of slow modulations of transequatorial thermal anomaly gradients dominated by the tropical north Atlantic. This is consistent with the Bjerknes (1964) hypothesis: quasi-decadal decreases (increases) in surface wind-stress in the North Atlantic tend to create reduced (enhanced) cross-equatorial wind that, through ocean dynamics and heat fluxes, could further generate warm (cold) SSTAs north (south) of the equator. Projection of the TW1 structure onto a 75-y SST dataset shows that such a time evolution is better observed over the last 20–30 y than before, except perhaps in the 1920 s and 1930s, but with shorter periods. The second Atlantic mode (TW2) expressing the statistical coupling between wind stress and SST anomalies is very different. Basically it points out in phase anomalies in the tropical Atlantic with stronger weights over the south-equatorial tropical Atlantic in northern summer. Its time series reflects an interannual variability dominated by higher frequencies with increased variance in the 1960s and 1970s until the recent post-1977 warming.

Correlations between the time coefficients of three selected oceanic indexes (TW1, TW2 and Nino3) and some basic NCEP/NCAR climate variables (surface air temperature, sea level pressure, moist static energy content at 850 hPa, precipitable water at the surface) have been investigated for the period 1968–1997 and over the 40 °N–40 °S; 120 °W–60 °E domain. TW1 and 2 can be thought as modes of regional extent (the strongest values concern only the Atlantic basin). Despite their statistical orthogonality (by construction) they are associated with climate anomaly patterns that denote an intensification of the meridional gradients in the near-equatorial zone due to higher wind-stress/SST interactions, the former mainly in OND and JFM in the northern basin, the latter from April to December in the near-equatorial zone. While these modes can be thought as influenced by the North Atlantic Oscillation (NAO) and the ENSO-Pacific variability in northern winter, their synchronous correlations with NAO, SOI and Nino3 are low and not significant (Table 1). The warm (cold) Pacific episodes are only slightly associated with warm (cold) SSTAs in the northern and southern parts of the tropical Atlantic. These correlations lead however to decreasing amplitude of thermal

anomalies in the tropical Atlantic. This could explain the nonstationarity of meridional anomaly gradients on seasonal and interannual time scales.

TW1 does not show by itself a clearly significant and persistent dipole signature (Figs. 2, 4) but only a weak antisymmetry primarily due to wind-stress / SST interactions in the north tropical Atlantic during the northern winter. However, when analyses convolve TW1 with ITCZ sensitive variables (temperatures, pressures, moist static energy, precipitable water) as in Figs. 6–9, one obtains dipole distributions meaning transequatorial anomaly gradients. These results denote thermodynamical processes at the ocean/atmosphere interface that create anomaly gradients in the meridional plane in a way, which tends to alter the mean seasonal cycle. This can produce abnormal excursions of the intertropical convergence zone (ITCZ) but appears to be consistent with the intrinsic non-dipole character of the tropical Atlantic surface variability at seasonal or annual time scale.

The seasonal modulation of continental rainfall at regional scale has been approached through NCEP/NCAR and observed rainfall indexes over the Nordeste region in Brazil, and the Guinea and Sahel zones in West Africa. When compared to the observations, the NCEP/NCAR indexes underestimate (overestimate) rainfall amounts in Nordeste and Guinea during their respective wet (dry) seasons. This diagnoses weaker seasonal and latitudinal amplitude of the simulated ITCZ and its associated rain band. However, the interannual rainfall variability in the model is rather well captured in Nordeste and Guinea.

Correlation and stratified analyses relative to those indices have shown moderate seasonal rainfall modulations linked to the Atlantic modes but significant connections when the two Atlantic modes + Nino3 were taken into account. This suggests that continental rainfall is particularly sensitive to some linear combinations of the three oceanic modes and hence to thermal forcing exerted by the resulting SSTA pattern. The warm (cold) Nino3 episodes are linked to drier (wetter) rainfall seasons in Nordeste and Sahel which however present significant links with TW1 and TW2, respectively. In fact the linear combinations involve always TW1 and TW2 (independent by construction) with opposite coefficients. Therefore we hypothesise that independent (quasi-random) fluctuations of TW1, TW2 and/or Nino3 can modify the transequatorial thermal, pressure and/or energy gradients in the vicinity of the ITCZ and thus exert significant surface forcings on rainfall amounts.

This can be simply illustrated through for example the NCEP/NCAR sea level pressure anomaly patterns relative to TW2 and Nino3 (Fig. 7 middle and bottom): the transequatorial gradients can be more easily created by a combination of type TW2 + Nino3 than by TW1 alone. TW2 + Nino3 are sufficient for generating a northward transequatorial anomaly gradient in sea level pressures over West Africa in northern summer and thus to oppose to the south-west monsoon penetration over the continent. In that context dry Sahelian situations tend to occur when warmer waters are present in the central-eastern Pacific and the Gulf of Guinea and hence when the maxima in tropical convergence are shifted equatorward.

Acknowledgements The authors are very grateful to David Enfield for his very helpful thought-provoking comments and to Michael Davey and an other anonymous reviewer who greatly improved the readability of the manuscript. They thank Mike Hulme (University of Norwich, England) for providing a recent version of the global analysed monthly precipitation dataset, and Jacques Servain (ORSTOM, Brest, France) for his monthly wind stress and SST data in the tropical Atlantic. They would like also to thank the United Kingdom Meteorological Office, the National Center for Atmospheric Research (USA) for providing respectively the global analysed monthly SST dataset and the NCEP/NCAR outputs, and, last but not least, Isabelle Poccard (University of Burgundy) for giving access to these data.

References

Bjerknes J (1964) Atlantic air–sea interaction. Adv Geophys, Academic Press, 1–82

Bottomley M, Folland CK, Hsiung J, Parker DE (1990) Global ocean surface temperature atlas. Meteorological Office and Massachusetts Institute of Technology, 313 plates

Bretherthon CS, Smith C, Wallace JM (1992) An intercomparison of methods for finding coupled patterns in climate data. J Clim 5:541–560

Carton J, Huang B (1994) Warm events in the tropical Atlantic. J Phys Oceanogr 24:888–903.

Carton JA, Cao X, Giese BS, Da Silva AM (1996) Decadal and interannual SST variability in the tropical Atlantic ocean. J Phys Oceanogr 26:1165–1175

Chang P (1996) The role of the dynamic ocean-atmosphere interactions in the tropical cycle. J Clim 9:2973–2985

Chang P, Li J, Li H (1997) A decadal climate variation in the tropical Atlantic Ocean from thermodynamic air–sea interactions. Nature 385:516–518

Curtis S, Hastenrath S (1995) Forcing of anomalous sea surface temperature evolution in the tropical Atlantic during Pacific warm events. J Geophys Res 100 C8:15 835–15 847

Delecluse P, Servain J, Levy C, Bengston L (1994) On the connection between the 1984 Atlantic warm event and the 1982–1983 ENSO. Tellus 46A:448–464

Druyan LM (1991) The sensitivity of Sub-Saharan precipitation to Atlantic SST. Clim Change 18:17–36

Enfield DB (1996) Relationships of inter-American rainfall to tropical Atlantic and Pacific SST variability. Geophys Res Lett 23:3305–3308

Enfield DB, Mayer D (1997) Tropical Atlantic sea surface temperature variability and its relation to the El Nino-Southern Oscillation. J Geophys Res 102 C1:929–945

Enfield DB, Metas-Nunez AM, Mayer DA, Cid-S L (1998) How ubiquitous is the dipole relationship in tropical Atlantic sea surface temperatures? Accepted in J Geophys Res (Oceans)

Folland CK, Palmer TM, Parker DE (1986) Sahel rainfall and worldwide sea temperature 1901–1985. Nature 320:602–607

Folland CK, Owen J, Ward MN, Colman A (1991) Investigation of seasonal rainfall in the Sahel region using empirical and dynamical methods. J Forecast 10:21–56

Fontaine B, Bigot S (1993) West African deficits and sea surface temperatures. Int J Climatol 13: 271–285

Fontaine B, Janicot S (1996) Sea surface temperature fields associated with west African rainfall anomaly types. J Clim 9: 2935–2940.

Fontaine B, Trzaska S, Janicot S (1998) Evolution of the relationship between near global Atlantic SST modes and the rainy season in West Africa: statistical analyses and sensitivity experiments. Clim Dyn 14: 353–368

Gill AE (1980) Some simple solutions for heat budget induced tropical circulation. Q J R Meteorol Soc 106: 447–463

Harzallah A, Rocha De Aragao JO, Sadourny R (1996) Interannual rainfall variability in Northeast: observation and model simulation. Int J Climatol 16: 861–878.

Hastenrath S (1984) Interannual variability and annual cycle: mechanisms of circulation and climate in the tropical Atlantic sector. Mon Weather Rev 112: 1097–1107

Hastenrath S (1990) Decadal scale changes of the circulation in the tropical Atlantic sector associated with Sahel drought. Int J Climatol 20:459–472

Hastenrath S, Greischar L (1993) Circulation mechanisms related to northeast Brazil rainfall anomalies. J Geophys Res (Atmos) 98: 5093–5102

Hastenrath S, Lamb PJ (1977) Climatic atlas of the tropical Atlantic and eastern Pacific Oceans, 97 charts, The University Wisconsin Press, Madison, USA

Houghton RW, Tourre YM (1992) Characteristics of low frequency sea surface temperature fluctuations in the tropical Atlantic. J Clim 5: 765–771

Huang B, Carton JA, Shukla J (1995) A numerical simulation of the variability in the tropical Atlantic ocean, 1980–88. J Phys Oceanogr 25: 835–854.

Hulme M, Jones PD (1993) A historical monthly precipitation data set for global land areas: application for climate monitoring and climate model evaluation. Analysis methods of precipitation on a global scale. Report of a GEWEX Workshop, 14–17 September 1992, Koblenz, WMO/TD 558, Geneva, pp A/14–A/17.

Janicot S, Moron V, Fontaine B (1996) Sahel droughts and ENSO dynamics. Geophys Res Lett 23(5): 515–518

Janicot S, Harzallah A, Fontaine B, Moron V (1998) West African monsoon dynamics and eastern equatorial Atlantic and Pacific SST anomalies (1970–1988). J Clim 11: 1874–1882

Kalnay E, Kanamitsu M, Kistler R, Collins W, Deaven D, Gandin L, Iredell M, Saha S, White G, Woollen J, Zhu Y, Chelliah M, Ebisuzaki W, Higgins W, Janowiak J, Mo KC, Ropelewski C, Wang J, Leetmaa A, Reynolds R, Jenne R., Joseph D (1996) The NCEP/NCAR 40 year reanalysis Project. Bull Am Meteorol Soc 77(3): 437–471

Kawamura R (1994) A rotated EOF analysis of global sea surface temperature variability with interannual and interdecadal scales. J Phys Oceanogr 24: 707–715

Lamb PJ (1978a) Case studies of tropical Atlantic surface circulation patterns during recent sub-Saharan weather anomalies: 1967 and 1968. Mon Weather Rev 106: 482–491

Lamb PJ (1978b) Large-scale tropical surface circulation patterns associated with sub-Saharan weather anomalies. Tellus 30: 240–251

Lamb PJ, Peppler RA (1992) Further case studies of tropical Atlantic surface atmospheric and oceanic patterns associated with sub-Saharan drought. J Clim 5: 476–488

Lanzante JR (1996) Lag relationships involving tropical sea surface temperature. J Clim 9: 2568–2578

Latif M, Kleeman R, Eckert C (1997) Greenhouse warming decadal variability or El Nino? An attempt to understand the anomalous 1990s. J Clim 10: 2221–2239

Lau K, Sheu PJ (1991) Teleconnections in global rainfall anomalies: seasonal to inter-decadal time scales. Glantz MH, Katz RW, Nicholls M (eds) Teleconnections linking worldwide climate anomalies, Cambridge University Press, pp 227–256

Lough JM (1986) Tropical Atlantic sea surface temperature and rainfall variations in subSaharan Africa. Mon Weather Rev 114: 561–570

Moron V, Bigot S, Roucou P (1995) Rainfall variability in subequatorial America and Africa and relationships with the main sea-surface temperature modes (1951–1990). Int J Climatol 15: 1297–1322

Moura AD, Shukla J (1981) On the dynamics of droughts in North-East Brazil: observations, theory and numerical experiments with a general circulation model. J Atmos Sci 38: 2653–2675.

Murakami M (1979) Large-scale aspects of deep convective activity over the Gate area Mon Weather Rev 107: 994–1013

Nobre P, Shukla J (1996) Variations of sea surface temperature, wind stress and rainfall over the tropical Atlantic and South America. J Clim 9: 2464–2479

Palmer TN (1986) The influence of the Atlantic, Pacific and Indian Oceans on Sahel rainfall. Nature 322: 251–253

Peixoto JP, Oort AH (1992) Physics of climate. American Institute of Physics, New York, 520pp.

Philander SGH (1990) El Nino, la Nina and the Southern Oscillation. In: Dmowska R, Holton JR (eds) International Geophysics Series 46 Academic Press, New York

Philander SGH, Gu D, Halpern D, Lambert G, Lau NC, Li T, Pacanowski RC (1996) Why the ITCZ is mostly north of the Equator. J Clim 9: 2958–2959

Ropelewski CF, Halpert MS (1987) Global and regional scale precipitation and temperature patterns associated with El Nino/Southern Oscillation. Mon Weather Rev 115: 1606–1626

Ropelewski CF, Halpert MS (1989) Precipitation patterns associated with the high index phase of the Southern Oscillation. J Clim 2: 268–284

Roucou P, Aragao JOB, Harzallah A, Fontaine B, Janicot S (1996) Vertical motion changes related to Northeast Brazil rainfall: AGCM simulation. Int J Clim 16: 879–892

Rowell DP, Folland CK, Maskell K, Ward N (1995) Variability of summer rainfall over tropical North Africa (1906–1992): observations and modelling. Q J R Meteorol Soc 113: 669–674

Semazzi FH, Burns B, Lin NH, Schemm JK (1996) A GCM study of teleconnections between the continental climate of Africa and global sea surface temperature anomalies. J Clim 9: 2480–2497

Semazzi FH, Mehta V, Sud YC (1988) An investigation of the relationship between sub-Saharan rainfall and global sea surface temperatures. Atmos-Ocean 26: 118–138

Servain J (1991) Simple climatic indices for the tropical atlantic Ocean. J Geophys Res, 96 C8: 15 137–15 146

Servain J, Picaut J, Busalacchi AJ (1985) Interannual and seasonal variability of the tropical Atlantic Ocean depicted by sixteen years of sea surface temperature and wind stress. In: Coupled ocean-atmosphere models. Elsevier Science Amsterdam, NL, pp 211–237

Shinoda M (1989) Annual rainfall variability and its inter-hemispheric coherence in the semi arid region of tropical Africa: data updated to 1987. J Meteorol Soc Japan 67: 555–564

Tanaka M, Weare W, Navato AR, Newell RE (1975) Recent African rainfall patterns. Nature 255: 201–203

Trenberth KE, Guillemot CJ (1998) Evaluation of the atmospheric moisture and hydrological cycle in the NCEP/NCAR reanalyses. Clim Dyn 14: 213–231

Trzaska S, Moron V, Fontaine B (1996) Global atmospheric response to specific linear combination of the main SST modes. Part I: numerical experiments and preliminary results. Ann Geophys 14: 1066–1077

Wagner R (1996) Mechanisms controlling variability of the inter-hemispheric sea surface temperature gradient in the tropical Atlantic. J Clim 9: 2010–2019

Wallace JM, Smith C, Bretherton CS (1992) Singular value decomposition of wintertime sea surface temperature and 500-mb height anomalies. J Clim 5: 561–576

Wallace JM, Zhang Y, Lau KH (1993) Structure and seasonality of interannual and interdecadal variability of the geopotential height and temperature fields in the Northern Hemisphere troposphere, J Clim 6 : 2063–2082

Ward MN (1992) Provisionally corrected surface wind data, worldwide ocean-atmosphere surface fields, and Sahelian rainfall variability. J Clim 5 : 454–475

Ward MN, Folland CK (1991) Prediction of seasonal rainfall in the Nordeste of Brazil using eigenvectors of sea-surface temperature. Int J Climatol 11 : 711–743

Ward MN, Folland CK, Maskell K, Rowell D, Colman A (1990) Understanding and predicting seasonal rainfall in sub-Saharan Africa. WMO, Tropical Meteorol Res Progr Rep Ser 36 : 157–161

Ward MN, Hoskins BJ (1996) Near-surface wind over the global ocean 1949–1988. J Clim 9 : 1877–1895

Wolter K (1989) Modes of tropical circulation, Southern Oscillation, and Sahel rainfall anomalies. J Clim 2 : 149–172

Zebiak S (1993) Air–sea interactions in the equatorial Atlantic region. J Clim 6 : 1567–1586